Fire Safety Journal 126 (2021) 103475

Contents lists available at ScienceDirect

Fire Safety Journal

journal homepage: www.elsevier.com/locate/firesaf

Subgrid-scale fire front reconstruction for ensemble coupled atmosphere-fire simulations of the FireFlux I experiment

Aurélien Costes [a,b,*], Mélanie C. Rochoux [a,**], Christine Lac [b], Valéry Masson [b]

[a] CECI, Université de Toulouse, CNRS, Cerfacs, 42 Avenue Gaspard Coriolis, 31100, Toulouse, France
[b] CNRM, Université de Toulouse, Météo-France, CNRS, 42 Avenue Gaspard Coriolis, 31100, Toulouse, France

ARTICLE INFO

Keywords:
Wildland fire
Fire spread
Fire weather
Blaze fire model
Level-set method
Heat flux parameterization
MesoNH atmosphere model
FireFlux I experiment

ABSTRACT

This paper introduces the Blaze fire model based on a Eulerian level-set front-tracking method and solved using high-order numerical schemes. Blaze includes an original and efficient subgrid-scale fire front reconstruction to substantially reduce computational cost and better localize surface heat fluxes compared to a weighted-averaged method. In this study, Blaze is coupled to the MesoNH atmospheric model to evaluate its performance against the FireFlux I experimental data set. Results show good agreement between simulations and measurements for both 25-m and 10-m atmospheric resolutions combined with a 5-m fire resolution. The fire-induced atmospheric flow below 10 m is correctly captured in the two-way coupled mode and leads to a realistic spread rate trend between the two instrumented towers compared to one-way forcing modes (forced and fire replay modes). A more realistic air temperature near the ground is obtained by considering heat fluxes in the already burnt area and not only at the flaming front. Also, the significant impact of inflow turbulence on both fire spread and fire-induced flow is highlighted. This study motivates the use of a statistical ensemble technique to account for near-surface turbulence and more generally, environmental variability at the scale of an experimental fire such as FireFlux I.

1. Introduction

Coupled atmosphere-fire modeling systems such as MesoNH-ForeFire [18,19,21], WRF-SFIRE [26,27,32] or WRF-FIRE [11,36] (the last two having evolved from CAWFE/Coupled Atmosphere-Wildland Fire Environment [6,13,14]) provide an efficient way to represent the behavior of a large-scale wildland fire by simultaneously solving for the fire spread, the plume updraft and their mutual interactions [12]. In this framework, the fire spread is represented as a moving front separating the burnt area from the unburnt vegetation using a parameterization of the front speed, called rate of spread, which takes as inputs surface wind conditions, biomass moisture content, biomass fuel properties and terrain topography [3,45,53]. The rate of spread is subject to significant uncertainties due to the simplified modeling approach [16] but also due to the limited knowledge in the inputs [43,44]. Coupling the fire spread model with an atmosphere model provides more realistic wind conditions as input to the fire spread model, which are known to be a key driver of the fire behavior [23,41].

The level-set (LS) method [39,49] is often used in front-tracking problems as an Eulerian formulation for interface transport. In wildland fire applications, it has been extensively used to propagate the time-evolving fire front [5,31,32,36,42,55], for instance in ELMFIRE [31] and SFIRE [32]. Bova et al. [5] have shown the equivalence of the LS method with Lagrangian markers, used for instance in FARSITE [22] and ForeFire [20], for standalone fire spread modeling. However, the LS formalism is particularly suited for coupling with atmosphere models such as MesoNH [29,30] or WRF [50]. An additional benefit of the LS is its ability to handle complex front geometry typical of wildfire events such as islands of unburnt fuel and merging fronts. The MesoNH-ForeFire system has, for instance, shown some scaling limitations when testing the atmospheric model sensitivity to mesh resolution and large-eddy simulation configuration. These limitations were partly due to the treatment of Lagrangian markers. To overcome this issue, a new fire model named Blaze has been developed to be easily embedded in atmospheric models and thereby design more efficient coupled atmosphere-fire modeling systems.

Blaze features two components: *i)* a spread component that propagates the fire front over time using a LS approach and given meteorological/environmental factors; and *ii)* a flux component that evaluates the surface latent/sensible heat fluxes released by the fire. When coupled with an atmospheric model, the fire model flux component

* Corresponding author. CECI, Université de Toulouse, CNRS, Cerfacs, 42 Avenue Gaspard Coriolis, 31100, Toulouse, France.
** Corresponding author.
E-mail addresses: aurelien.costes@cerfacs.fr (A. Costes), melanie.rochoux@cerfacs.fr (M.C. Rochoux).

https://doi.org/10.1016/j.firesaf.2021.103475
Received 31 August 2020; Received in revised form 18 July 2021; Accepted 7 October 2021
Available online 14 October 2021

Abbreviation

2WC	two-way coupling mode
A*x* F*y*	simulation with *x*-m resolution for the atmospheric model and *y*-m resolution for the fire model
A2F	atmosphere-to-fire coupling mode
AGL	above ground level
ASE	available sensible energy
AWC	available water content
CST	constant flux parameterization
EFFR	explicit fire front reconstruction
ENO	essentially non oscillatory
EXS	exponential-smoldering flux parameterization
F2A	fire-to-atmosphere coupling mode
LS	level-set
LT	local time
PPM	piecewise parabolic method
RK	Runge-Kutta
WA	weighted average
WENO	weighted essentially non oscillatory

Superscript

n	time index

Subscript

(x, y)	2-D cartesian coordinates
d	dead fuel
h	sensible heat
i	fire mesh index in the x-direction
j	fire mesh index in the y-direction
l	live fuel
w	latent heat

Symbol

c_{pa}	air calorific capacity
c_{pd}	fuel calorific capacity
$\mathcal{C}$	case identifier in level-set reconstruction method
d	intersection quantity in level-set reconstruction method
e	fuel layer thickness
E_c	combustion efficiency
LAI	leaf area index
M	fuel moisture content
$\mathbf{n}$	fire front normal vector
r	Pearson correlation
r_{00}	radiant heat transfer parameter
$\mathcal{R}$	rate of spread
$\mathcal{R}_0$	rate of spread without wind and slope
s	fuel particle surface-area-to-volume ratio
s_t	stochiometric mass-based air/fuel ratio
$\mathcal{S}$	subgrid burning area
t	time
T_a	air temperature
T_i	ignition temperature
t^a	fire arrival time
α_f	fraction of energy released during flaming phase
Γ	fire mesh refinement ratio
Δh	water evaporation enthalpy
ΔH	combustion enthalpy
Δx	atmospheric horizontal mesh size
Δx_f	fire mesh size
$\widetilde{\Delta}$	modified Laplacian operator
ρ_a	air density
ρ	fuel particle mass density
σ	fuel surface load
ϵ_φ	diffusion coefficient for level-set function
λ	stiffness parameter in level-set reconstruction method
∇	gradient operator
τ_0	residence time parameter
τ_f	fire residence time
τ_e	characteristic time of exponential-smoldering flux parameterization
φ	level-set function
ψ	flux parameterization in fire model

imposes latent and sensible heat fluxes as surface boundary conditions to the atmosphere model, while the atmosphere model imposes the surface wind field as input to the fire model spread component. To make this coupling more computationally efficient, Blaze includes an original LS approach based on a subgrid-scale explicit fire front reconstruction (EFFR) method.

The observational datasets to evaluate coupled fire-atmosphere models have mainly been collected through experimental fires [40], among whom RxCADRE [37] and FireFlux [7,10] field campaigns. One advantage of experimental fires as compared to active wildfires is the ability to control environmental conditions, even though it remains difficult to characterize initial and boundary conditions. One drawback is that the burning conditions (e.g. low wind, relatively flat terrain) are not fully representative of actual uncontrolled wildfires. FireFlux experiments corresponding to experimental fires in homogeneous grass fields were specifically designed to measure quantities of interest at the scale of the atmospheric boundary layer, in order to provide the first observational datasets on the fire-induced meteorology. The 2006 FireFlux I experiment was a wind-dominated fire and was therefore used to validate WRF-SFIRE [26] and MesoNH-ForeFire [21]. For comparative purposes, the FireFlux I experiment is used in the present study as a first validation step of the Blaze fire model.

In this work, Blaze is coupled with an atmospheric model in large-eddy simulation mode to simulate turbulent flows and to have a realistic representation of the atmospheric boundary layer. Several coupling modes between Blaze and the atmospheric model are available to provide a flexible way to analyze the interactions between the different components of the coupled atmosphere-fire model. One-way coupling modes are of primary importance to study the forcing impact on the fire model and the atmospheric model in a separate way. The atmosphere-to-fire (A2F) mode gives insights into the atmospheric model forcing on the fire spread model without considering fire feedback on the atmosphere. Reciprocally, the fire-to-atmosphere (F2A) mode, also known as the fire replay mode in the literature [33], gives insights into the fire spread model forcing on the fire flux model component and on the micro-scale atmospheric fields without considering atmospheric feedback on the fire spread. Sensitivity tests with respect to the fire model resolution are performed to show Blaze convergence in terms of fire front location on the one hand, and in terms of heat flux intensity and distribution on the other hand. The benefits of the EFFR method to represent surface heat fluxes are highlighted with respect to the LS weighted average method, which is for instance implemented in WRF-SFIRE to reconstruct the burning area. A two-way coupled (2WC) mode is finally used to highlight the impact of the fire-induced meteorology on the wildland fire behavior. For all coupling modes, ensembles of coupled atmosphere-fire simulations are carried out to study the influence of inflow turbulence on the wildland fire behavior.

The outline of the paper is as follows. The Blaze fire model is described in Section 2. The atmosphere-fire coupling strategies available in Blaze are presented in Section 3. Section 4 presents the simulation

experiments used for Blaze evaluation, involving the MesoNH atmospheric model and the FireFlux I experimental dataset (referred to as FireFlux in the following). Results in one- and two-way coupling modes for different fire model resolutions and different atmospheric model resolutions are discussed in Section 5.

2. The Blaze fire model

The Blaze fire model features the following components: an Eulerian two-dimensional front-tracking model that relies on a LS method and uses a description of the local rate of spread based on Balbi's formulation [3]; and a flux parameterization that estimates the spatial distribution and intensity of the surface latent and sensible heat fluxes. If Blaze is embedded in an atmospheric model, these heat fluxes act as surface boundary conditions to solve the atmospheric flow perturbed by the fire.

2.1. Level-set method for fire front tracking

2.1.1. Governing equation

The LS method is used to propagate the time-evolving fireline on a two-dimensional horizontal plane (x, y). The two-dimensional fire grid is defined with respect to the resolution of the atmospheric data. Since the fireline propagation is a subgrid-scale process with respect to the atmosphere, the atmospheric mesh is divided into Γ_x cells in the x-direction and Γ_y cells in the y-direction to form the fire mesh in Blaze. A distinction is therefore made between the atmospheric surface mesh, referred to as "atmospheric mesh", of resolution $(\Delta x, \Delta y)$, and the fire mesh of resolution $(\Delta x_f, \Delta y_f)$ with $\Delta x_f = \Delta x/\Gamma_x$ and $\Delta y_f = \Delta y/\Gamma_y$.

In Blaze, the LS function $\varphi \equiv \varphi(x, y, t)$ is not a signed distance but rather a bounded function $0 \leqslant \varphi \leqslant 1$, where the contour line $\varphi = 0.5$ is identified as the fire front; $\varphi > 0.5$ represents burnt vegetation; and $\varphi < 0.5$ represents unburnt vegetation at a given time t. The LS field is transported at the rate of spread $\mathcal{R}$ and satisfies the following Hamilton-Jacobi equation:

$$\frac{\partial \varphi}{\partial t} = \mathcal{R}(|\nabla \varphi| + \varepsilon_\varphi \widetilde{\Delta}\varphi) \tag{1}$$

where $\nabla\varphi = \left(\frac{\partial\varphi}{\partial x}, \frac{\partial\varphi}{\partial y}\right)$ is the LS gradient, $\widetilde{\Delta}\varphi = \left(\Delta x_f \frac{\partial^2\varphi}{\partial x^2} + \Delta y_f \frac{\partial^2\varphi}{\partial y^2}\right)$ is the fire-mesh-size-proportional Laplacian, $\varepsilon_\varphi \widetilde{\Delta}\varphi$ is the artificial viscosity term to ensure numerical stability, and $\mathcal{R}$ represents the speed projected onto the normal direction $\mathbf{n}$ to the fireline, $\mathbf{n} = -\nabla\varphi/|\nabla\varphi|$. $\mathcal{R}$ is evaluated using Balbi's rate-of-spread parameterization (Section 2.2).

2.1.2. Numerics

In Blaze, numerical tests have shown that $\varepsilon_\varphi = 0.1$ is sufficient to obtain a satisfactory solution for smooth spatial distribution of fuel properties consistently with Muñoz-Esparza et al. [36]. Numerical viscosity is also applied to the rate of spread to prevent from oscillations at the fire flanks due to atmospheric turbulence. It is worth noting that in WRF-SFIRE, Mandel et al. [32] recommended to use $\varepsilon_\varphi = 0.4$. This aspect will be important to investigate for heterogeneous fuel properties and high spatial variation of the rate of spread. However, this is beyond the scope of the present FireFlux experiment that is limited to a homogeneous grass fuel (Section 4.2).

Mandel et al. [32] initially implemented in WRF-SFIRE a second-order explicit RK (Runge-Kutta) scheme for time integration combined with first-order ENO (Essentially Non-Oscillatory) [38] scheme (RK2-ENO1). Muñoz-Esparza et al. [36] demonstrated that a high-order LS method using third-order explicit RK scheme combined with third-order WENO (Weighted Essentially Non-Oscillatory) [25] scheme (RK3-WENO3) is efficient and much more accurate than RK2-ENO1. For this purpose, Eq. (1) is solved in Blaze using RK3-WENO3.

2.1.3. Burning map

Equation (1) is solved sequentially over the duration of the wildland fire. The resulting time-evolving fireline position is concatenated into an arrival time map. The arrival time $t^a \equiv t^a(x, y)$ is defined at the center of each fire cell and is defined by the time at which the LS function exceeds 0.5. The arrival time map is initialized at -1, meaning that no fire is in the domain. Ignition occurs and the arrival time map is iteratively updated. For a given fire cell (x, y), at time t indexed by n, a negative arrival time means that the fire has not yet reached the center of the fire cell (i.e. $t^{a,n} = -1$ and $\varphi^n < 0.5$). Consider the fire front has reached the fire cell at time $(t + \Delta t)$ indexed by $(n + 1)$, i.e. $\varphi^{n+1} \geqslant 0.5$. Then, the arrival time $t^{a,n+1}$ for the fire cell (x, y) is estimated using linear interpolation between time t and time $(t + \Delta t)$. As the arrival time map t^a is a cumulative field, once the arrival time is calculated for a given fire cell (x, y), it cannot change. The arrival time map is referred to as the burning map in the following.

2.2. Rate-of-spread parameterization

In this work, for consistency purpose with previous MesoNH-ForeFire studies, we follow the choices made by Filippi et al. [21]. The rate of spread $\mathcal{R}$ is evaluated using Balbi's parameterization [3], which was adapted by Santoni et al. [48] to landscape-scale problem and used for instance to simulate wildland fires in the Mediterranean area [18,52]. Balbi's formulation is detailed in Appendix A.

Similarly to the well-known Rothermel's formulation [45], the Balbi's formulation is a parametric function of the rate of spread given terrain slope, surface wind speed, biomass moisture content and biomass fuel parameters. The list of the required input parameters is given in Table 4. There are two main differences between Balbi's and Rothermel's formulations. On the one hand, Balbi's formulation is based on mass, momentum and energy conservation, while Rothermel's one is only based on energy conservation. In Balbi's formulation, assumptions are made on the geometrical and thermodynamical properties of the flame to obtain a simplified rate-of-spread formulation at any point on the fire front. On the other hand, Balbi's formulation provides a varying no-wind rate of spread along the flanks and at the back of the fire even if the vegetation is homogeneous. This is not the case for Rothermel's formulation, whose constant no-wind rate of spread can become an issue to properly track the fire front propagation [26,35].

In the present study, the near-surface wind conditions required as inputs to the rate-of-spread parameterization are derived from simulated atmospheric data at a constant height (Section 3). Kochanski et al. [28] showed that there is no clear relationship between the vertical resolution of the first atmospheric level and the surface wind at the fire level. For this reason, the surface wind conditions are given in Blaze at 2-m above ground level (AGL). They are then interpolated horizontally using two-dimensional bilinear interpolation with a twelve-point stencil. This aspect of the wind interpolation height will be important to investigate if there are some spatial variation of the vegetation height throughout the computational domain [56], but this is not necessary for the FireFlux case study.

2.3. Surface heat flux parameterization

Blaze provides an estimation of the sensible and latent heat fluxes at the surface, which can be seen as diagnostic variables of the fire model and which can be injected in an atmospheric model in the framework of coupled atmosphere-fire simulations. From an atmospheric model viewpoint, the fire is only represented as surface heat fluxes. This is why their description in terms of location and intensity is of first importance in coupled mode.

2.3.1. Energy reservoirs

The heat flux computation in Blaze is based on the concept of energy reservoirs. These reservoirs determine the amount of latent and sensible

energy that is available in the vegetation and that can be injected from the surface into the atmosphere. The available water content (AWC) relates to the latent heat that can be transferred to the atmosphere due to water evaporation. The available sensible energy (ASE) relates to the sensible heat that can be transferred due to combustion. For each fire cell, the AWC and ASE quantities are initially estimated from biomass fuel parameters (Table 4) derived from [19,32,35].

$$\mathrm{AWC}^0 = \sigma_d\, M_d + \sigma_l\, M_l \tag{2}$$

$$\mathrm{ASE}^0 = \frac{(E_c + E_s)\,(1-\chi_0)\,\sigma_d\,\Delta H}{1+M_d} \tag{3}$$

where the default values for the flaming combustion efficiency (E_c = 0.75) and the radiant heat transfer fraction (χ_0 = 0.3) are used [21], where the total energy release due to smoldering processes is zero (E_s = 0) if only the flaming phase of the fire is considered, and where the remaining fuel parameters are based on FireFlux field data (Section 4.2).

When the fire propagates, the energy released between time t and time $(t + \Delta t)$ is removed from the AWC and ASE reservoirs as follows:

$$\mathrm{AWC}^{n+1} = \mathrm{AWC}^n - \Delta t\, \mathcal{S}^n\, \psi_w^n \tag{4}$$

$$\mathrm{ASE}^{n+1} = \mathrm{ASE}^n - \Delta t\, S^n\, \psi_h^n \tag{5}$$

where Δt is the fire model time step, $\mathcal{S}^n$ is the fraction of the fire cell that is currently burning, and ψ_w^n (ψ_h^n) is the fire cell contribution to the released latent (sensible) heat flux. The calculation of $\mathcal{S}^n$ is detailed in Section 2.3.2, and the calculation of both ψ_w^n and ψ_h^n is detailed in Section 2.3.3.

When the energy that should be released between t and $(t + \Delta t)$ is larger than the energy remaining in the reservoir (i.e. $\mathrm{AWC}^n < \Delta t\, \mathcal{S}^n\, \psi_w^n$ for latent heat), then the heat flux intensity is adjusted to have an empty reservoir at time $(t + \Delta t)$ (i.e. $\psi_w^n = \frac{\mathrm{AWC}^n}{\mathcal{S}^n\,\Delta t}$). When the reservoir is empty (i.e. $\mathrm{AWC}^n = 0$), the heat flux intensity is zero (i.e. $\psi_w^n = 0$). The same approach applies to ASE.

From the perspective of the atmospheric model, the heat flux contribution to a given atmospheric cell at a given time is calculated as the average of the heat fluxes computed for all fire cells contained in the atmospheric cell.

2.3.2. Explicit fire front reconstruction method

To compute latent and sensible heat fluxes at a given time in Eqs. (4) and (5), the fraction of the fire cell that is currently burning ($\mathcal{S}^n$) is required. The method to estimate this quantity $\mathcal{S}^n$ for each fire mesh cell is detailed here. For clarity purpose, the time index n is dropped in this section.

In WRF-SFIRE, the subgrid-scale burning area is estimated through a weighted average of the LS [32] on a nine-point stencil around the considered fire cell (i, j) as follows:

$$\begin{aligned}\mathcal{S} \equiv \mathcal{S}_{i,j} = \; & \frac{9}{16}\varphi_{i,j} + \frac{3}{32}\left(\varphi_{i-1,j} + \varphi_{i,j-1} + \varphi_{i+1,j} + \varphi_{i,j+1}\right) + \\ & \frac{1}{64}\left(\varphi_{i-1,j-1} + \varphi_{i+1,j-1} + \varphi_{i+1,j+1} + \varphi_{i-1,j+1}\right)\end{aligned} \tag{6}$$

One limitation of this approach, referred to as the weighted average (WA) method in the following, is that its accuracy depends on the numerical diffusion of the fire front. The quality of the subgrid-scale burning area estimation is then closely related to the quality of the LS advection discretization and of the mesh resolution.

To overcome this limitation, the fire front is explicitly reconstructed within the fire cell using the EFFR method in Blaze. The key idea is to map the contour line $\varphi = 0.5$ inside the fire cell partitioned into four quadrants ($\mathcal{S}_1$ to $\mathcal{S}_4$ in Fig. 1). This is done in two steps. A first step identifies the intersections between the quadrant faces and the contour line $\varphi = 0.5$. A second step represents the fire front as straight line

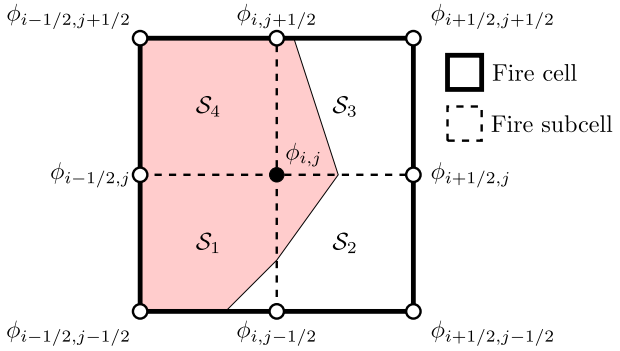

Fig. 1. Schematic of the subgrid-scale burning area computation (red area) in a given fire cell (thick solid line) divided into four quadrants, or fire subcells, $\mathcal{S}_1$ to $\mathcal{S}_4$ (dashed straight lines). The thin solid line represents the reconstructed fire front through the EFFR method. (For interpretation of the references to color in this figure legend, the reader is referred to the Web version of this article.)

between these intersections and derives the subgrid burning area in each of the four quadrants by only considering triangles and trapezes (red areas in Fig. 1).

In the first step, the LS function is interpolated at each corner of a given quadrant to estimate the quantities $\{\varphi_1, \varphi_2, \varphi_3, \varphi_4\}$ (see Table 2 for notations). The associated intersection quantities $\{d_1, d_2, d_3, d_4\}$ are computed as

$$d_1 = sgn\left(\frac{1}{2}, \varphi_1 - \frac{1}{2}\right) - sgn\left(\frac{1}{2}, \varphi_2 - \frac{1}{2}\right) \tag{7}$$

$$d_2 = sgn\left(\frac{1}{2}, \varphi_2 - \frac{1}{2}\right) - sgn\left(\frac{1}{2}, \varphi_3 - \frac{1}{2}\right) \tag{8}$$

$$d_3 = sgn\left(\frac{1}{2}, \varphi_4 - \frac{1}{2}\right) - sgn\left(\frac{1}{2}, \varphi_3 - \frac{1}{2}\right) \tag{9}$$

$$d_4 = sgn\left(\frac{1}{2}, \varphi_1 - \frac{1}{2}\right) - sgn\left(\frac{1}{2}, \varphi_4 - \frac{1}{2}\right) \tag{10}$$

where $\mathrm{sgn}(a, b)$ returns a with the sign of b. The possible values for the intersections quantities are then −1, 0 and 1. Table 1 gives an example of the possible intersection values for d_1. Intersection quantities indicate if there is an intersection (non-zero values) but also where the LS function is above 0.5 (positive or negative values).

In the second step, a case identifier denoted by $\mathcal{C}$ is derived from intersection quantities as follows:

$$\mathcal{C} = 3^0(1+d_1) + 3^1(1+d_2) + 3^2(1+d_3) + 3^3(1+d_4). \tag{11}$$

$\mathcal{C}$ provides a way to identify the different fire front geometric configurations, and each identified case $\mathcal{C}$ has its specific area estimation $\mathcal{S}_\mathcal{C}$. In practice, only three equations are required to consider all possible cases:

$$\mathcal{S}_{68}(\varphi_1, \varphi_2, \varphi_3, \varphi_4) = \frac{(0.5-\varphi_1)^2}{2(\varphi_2-\varphi_1)(\varphi_4-\varphi_1)} \tag{12}$$

$$\mathcal{S}_{70}(\varphi_1, \varphi_2, \varphi_3, \varphi_4) = \frac{1}{2}\left[\frac{(0.5-\varphi_1)}{\varphi_4-\varphi_1} + \frac{0.5-\varphi_2}{\varphi_3-\varphi_2}\right] \tag{13}$$

Table 1
Possible values for the intersection quantity d_1 in a fire cell quadrant given the interpolated LS function at the corners $\{\varphi_1, \varphi_2\}$ – EFFR method.

d_1	$\varphi_1 < 0.5$	$\varphi_1 \geqslant 0.5$
$\varphi_2 < 0.5$	0	1
$\varphi_2 \geqslant 0.5$	−1	0

$$\mathcal{S}_{22}(\varphi_1,\varphi_2,\varphi_3,\varphi_4)=\frac{-(\varphi_4-0.5)^2}{2(\varphi_4-\varphi_1)(\varphi_3-\varphi_4)}. \quad (14)$$

The area for the other cases is obtained by combining or permuting previous formulas. Each case implemented in Blaze is given in Table 2. Note that case 56 is complementary to case 24 in identifier but the formulas are not. Indeed, the complementary area of case 24 is less realistic than the one of case 56 with two separated fronts in the same quadrant. This approach is applied for each of the four quadrants of a given fire cell. The subgrid burning area of the fire cell $\mathcal{S}$ is finally obtained by averaging the burning area obtained for each of the four quadrants of the fire cell:

$$\mathcal{S}=\frac{1}{4}(\mathcal{S}_1+\mathcal{S}_2+\mathcal{S}_3+\mathcal{S}_4) \quad (15)$$

2.3.3. Surface heat flux formulation

To compute latent and sensible heat fluxes at a given time in Eqs. (4) and (5), the time-varying flux intensity denoted by ψ_w^n for latent heat flux and ψ_h^n for sensible heat flux is required. The formulation of these quantities ψ_w^n and ψ_h^n is given in this section. Different parameterizations that only depend on time, the fire arrival time and the biomass fuel properties are available in Blaze. The CST and EXS flux parameterizations used in this study are briefly described here and are summarized in Table 3.

Constant flux parameterization (CST) In previous studies [19,21], heat fluxes only accounted for the flaming phase of the fire, meaning that heat fluxes were only injected into the atmospheric model at the fire arrival time and during a characteristic time called the flaming residence time τ_f [1]. This approach is referred to as the constant flux parameterization (CST). It consists of releasing a constant heat flux until the energy reservoir is empty.

Table 2
Overview of all possible fire front configurations in Blaze: each configuration is identified by $\mathcal{C}$ and the corresponding quadrant subgrid burning area $\mathcal{S}_\mathcal{C}$ is obtained by interpolating the LS function at the four quadrant corners $\{\varphi_1, \varphi_2, \varphi_3, \varphi_4\}$ – EFFR method.

Case	$\mathcal{C}$	$\mathcal{S}_\mathcal{C}$	Case	$\mathcal{C}$	$\mathcal{S}_\mathcal{C}$
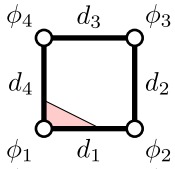	68	$\mathcal{S}_{68}(\varphi_1,\varphi_2,\varphi_3,\varphi_4)$	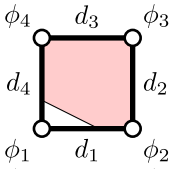	12	$1-\mathcal{S}_{68}(\varphi_1,\varphi_2,\varphi_3,\varphi_4)$
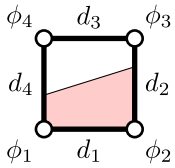	70	$\mathcal{S}_{70}(\varphi_1,\varphi_2,\varphi_3,\varphi_4)$	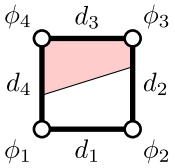	10	$1-\mathcal{S}_{70}(\varphi_1,\varphi_2,\varphi_3,\varphi_4)$
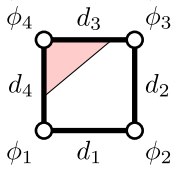	22	$\mathcal{S}_{22}(\varphi_1,\varphi_2,\varphi_3,\varphi_4)$	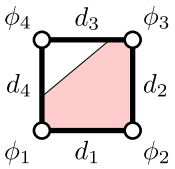	58	$1-\mathcal{S}_{22}(\varphi_1,\varphi_2,\varphi_3,\varphi_4)$
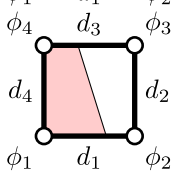	50	$\mathcal{S}_{70}(\varphi_1,\varphi_4,\varphi_3,\varphi_2)$	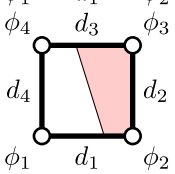	30	$1-\mathcal{S}_{70}(\varphi_1,\varphi_4,\varphi_3,\varphi_2)$
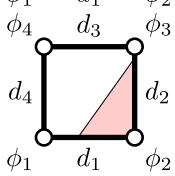	42	$\mathcal{S}_{22}(\varphi_1,\varphi_4,\varphi_3,\varphi_2)$	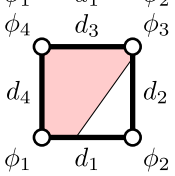	38	$1-\mathcal{S}_{22}(\varphi_1,\varphi_4,\varphi_3,\varphi_2)$
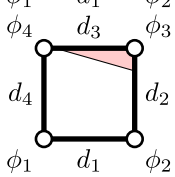	28	$\mathcal{S}_{68}(\varphi_3,\varphi_2,\varphi_1,\varphi_4)$	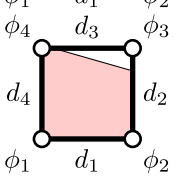	52	$1-\mathcal{S}_{68}(\varphi_3,\varphi_2,\varphi_1,\varphi_4)$
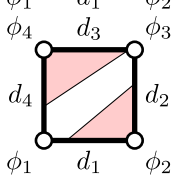	24	$\mathcal{S}_{22}(\varphi_1,\varphi_2,\varphi_3,\varphi_4)+\mathcal{S}_{22}(\varphi_1,\varphi_4,\varphi_3,\varphi_2)$	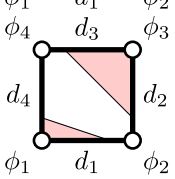	56	$\mathcal{S}_{68}(\varphi_1,\varphi_2,\varphi_3,\varphi_4)+\mathcal{S}_{68}(\varphi_3,\varphi_2,\varphi_1,\varphi_4)$

Table 3
Latent and sensible heat flux parametrizations in Blaze.

Heat flux	Equation	Parameters (default value)	Flaming phase modeling	Smoldering phase modeling	time dependant
Constant parametrization (CST)					
Latent	$\psi_w^{\mathrm{CST}}(t,t^a) = \frac{\mathrm{AWC}^0}{\tau_f}$		✓	×	×
Sensible	$\psi_h^{\mathrm{CST}}(t,t^a) = \frac{\mathrm{ASE}^0}{\tau_f}$	$E_s = 0$	✓	×	×
Exponential and smoldering parametrization (EXS)					
Latent	$\psi_w^{\mathrm{EXS}}(t,t^a) = \psi_{w,e}\, e^{-\frac{t-t^a}{\tau_e}}$	$\alpha_f = 0.8$	✓	×	✓
Sensible	$\psi_h^{\mathrm{EXS}}(t,t^a) = \psi_{h,e}\, e^{-\frac{t-t^a}{\tau_e}} + \psi_s$	$\alpha_f = 0.8$ $E_s = 0.15$	✓	✓	✓
$\psi_{h,e} = \frac{\mathrm{ASE}^0}{\tau_e}$	$\psi_{w,e} = \frac{\mathrm{AWC}^0}{\tau_e}$	$\tau_e = -\frac{\tau_f}{\ln(1-\alpha_f)}$	$\psi_s = \frac{0.009\ \mathrm{ASE}^0}{\tau_f}$		

Table 4
Definition and numerical value of parameters used as inputs to the Balbi's rate-of-spread formulation (for the biomass fuel parameters, the subscript "d" corresponds to 1-h dead fuel and the subscript "l" corresponds to thin live fuel).

Symbol	Definition	Value	Unit
c_{pd}	Fuel calorific capacity	1,912	J K^{-1} kg^{-1}
c_{pa}	Air calorific capacity	1,004	J K^{-1} kg^{-1}
e	Fuel layer thickness	1.5	m
E_c	Combustion efficiency	0.75	–
LAI	Leaf area index	4	–
M_d	Fuel moisture content	9	%
M_l		200	
r_{00}	Radiant heat transfer parameter	2.5×10^{-5}	m s^{-1}
s_d	Fuel particle surface-area-to-volume ratio	4,446	m^{-1}
s_l		4,446	
s_t	Stoichiometric mass-based air/fuel ratio	8.3	–
T_a	Air temperature	291	K
T_i	Ignition temperature	590	K
χ_0	Radiant heat transfer fraction	0.3	–
Δh	Water evaporation enthalpy	2.5	MJ kg^{-1}
ΔH	Combustion enthalpy	15.43	MJ kg^{-1}
ρ_a	Air density	1.2	kg m^{-3}
ρ_d	Fuel particle mass density	400	kg m^{-3}
ρ_l		400	
σ_d	Fuel surface load	1.04	kg m^{-2}
σ_l		0.04	
τ_0	Residence time parameter	75,590	m^{-1} s

Exponential flaming-smoldering parameterization (EXS) For coupled atmosphere-fire simulations, accounting for the temporal variability of the heat flux may be important to represent the fire dynamic behavior as done in WRF-SFIRE [32]. Accounting for the sensible heat released behind the fire front (i.e. the smoldering phase of the fire) may also be important to capture the fire influence on the surrounding atmosphere by preheating the air entrained towards the fire front. These two effects are accounted for in Blaze through the exponential flaming-smoldering parameterization (EXS). An exponential decay of the latent and sensible heat fluxes is considered through the characteristic time $\tau_e = -\tau_f/\ln(1-\alpha_f)$. The input parameter $0.5 \leqslant \alpha_f < 1$ represents the fraction of the total energy at the initial time (AWC^0 for latent heat and ASE^0 for sensible heat) that is released during the flaming residence time τ_f. Smoldering effects are accounted for in two ways. First, they impact the total energy release (ASE^0 in Eq. (3) with $E_s = 0.15$). Second, they contribute to the sensible heat flux, the smoldering contribution ψ_s is given as a fraction (0.9%) of the nominal sensible heat flux used in CST parameterization. It is worth noting that the smoldering contribution remains small in the present study since the smoldering effects are limited for grass fuels typical of the FireFlux experiment. This aspect will be important to revisit when considering other biomass fuels than grass.

Vertical flux distribution Once computed at the surface, the average value of the heat fluxes over a given atmospheric grid Ψ[W m^{-2}]is vertically distributed using an exponential decay $\mathcal{F}(z)\ [\mathrm{W\,m^{-3}}] = F_0 \exp(z/z_f)$ in order to integrate heat fluxes directly in the corresponding prognostic equations of MesoNH. The term $\mathcal{F}_0$ is computed by

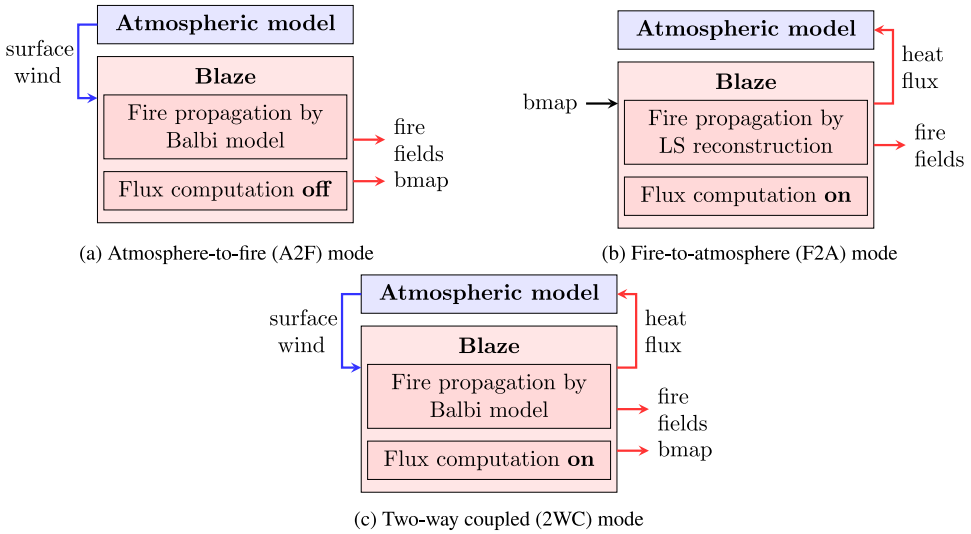

Fig. 2. Schematics of Blaze coupling modes (bmap corresponds to the burning map defined in Section 2.1.3).

imposing the constraint $\int_0^{z_{max}} \mathcal{F}(z)\,dz = \Psi$, with z_f and z_{max} the two parameters of the vertical flux distribution.

3. Coupling strategy

This section presents the three coupling modes between Blaze and an atmospheric model that are used in this work. For each mode, the coupling variables are exchanged at each atmospheric time step.

3.1. Forced atmosphere-to-fire mode (forced mode)

In the forced (A2F) mode (Fig. 2a), the fire spread is affected by the atmospheric flow but the wind conditions are not disturbed by the fire. Blaze requires the wind conditions near the surface from an atmospheric model to compute the Balbi's rate of fire spread but no heat flux computation is needed. As output, Blaze provides the burning map and the fire related fields (LS function φ, rate of spread $\mathcal{R}$, wind contribution to the rate of spread $(\mathcal{R} - \mathcal{R}_0)$, ASE and AWC).

3.2. Forced fire-to-atmosphere mode (fire replay mode)

To perform numerical convergence tests or investigate the atmospheric response to fire energy release, it is of primary interest to run simulations from a predetermined fire. This fire replay (F2A) mode (Fig. 2b) takes as input an existing burning map (obtained from simulation or observation), and computes latent and sensible heat fluxes to be injected into the atmospheric model. The fire spread model component is not used. Instead, a temporal reconstruction of the LS function φ is performed from information contained in the burning map. This is done through a sigmoid function of parameter λ:

$$\varphi(x,y,t) = \frac{1}{1+e^{-\lambda(t-t^a(x,y))}} \tag{16}$$

where the stiffness parameter λ [s^{-1}] corresponds to the numerical spread of the LS function that would be obtained by integrating Eq. (1) using RK3-WENO3 numerical schemes. This is important to reconstruct a realistic LS field from the burning map to then force the atmosphere model.

In the present study, λ is assumed to be uniform in the domain but dependent on the fire mesh size Δx_f. Several Blaze simulations run on a simplified test case (Appendix B) have shown that λ is given by the following law with respect to Δx_f:

$$\lambda(\Delta x_f) = 2.136\, e^{-0.211(\Delta x_f + 8.613)} + 0.064 \tag{17}$$

for $1 \leqslant \Delta x_f \leqslant 25$ [m]. This reconstruction leads to maximum error between reconstructed LS and original LS lower than 9% for the coarsest mesh and lower than 0.5% for the most refined mesh. Most importantly, the sigmoid formulation (Eq. (16)) guarantees by definition the exact same fire front position represented by the contour line $\varphi = 0.5$. The injected heat fluxes are thereby well reproduced in the F2A simulations compared to the original simulations carried out in two-way coupled mode for varying fire mesh resolution Δx_f.

3.3. Two-way coupled mode

The 2WC (Fig. 2c) accounts for the two-way interactions between the fire model and the atmospheric model, meaning that surface winds simulated by the atmosphere model are used as input to the fire spread model component and that the fire feedback onto the atmosphere is imposed through the surface latent and sensible heat flux model components in Blaze.

4. Verification and validation

4.1. MesoNH-Blaze coupled system

In this study, Blaze is coupled with the MesoNH [30,29] atmosphere model. MesoNH, developed by both Météo-France and Laboratoire d'Aérologie, is a non-hydrostatic anelastic atmosphere model. MesoNH is used to simulate meso-scale (kilometric resolution) up to micro-scale (metric resolution) atmospheric flows [2,4,18,46,47,54]. To numerically solve Navier-Stokes equations, MesoNH uses a five-stage third--order explicit RK scheme (RK53) for time integration associated with a fifth-order WENO scheme (WENO5) for wind advection and the piecewise parabolic method (PPM) for meteorological variables and tracer advection [15]. An explicit 3-D turbulence scheme [17] is used with a mixing length given by the grid size. MesoNH is run in idealized configurations. Initially, turbulence is generated by adding a random potential temperature perturbation at the first vertical level of the atmosphere. A spin-up is then run to establish turbulence in the computational domain. Lateral boundary conditions are cyclic to enhance turbulence. High-altitude winds are provided by geostrophic forcing. Blaze forces the MesoNH atmospheric model through the external land surface platform SURFEX [34]; in SURFEX the land cover and the surface parameters are provided by the ECOCLIMAP database [57]. Due to the limited physical time that is simulated by MesoNH-Blaze in this work, the radiative scheme in Meso-NH is not activated.

In this study, the focus is made on analyzing the interactions between Blaze and an atmospheric model when the flow is turbulent to be representative of actual atmospheric conditions during wildland fires. Before considering turbulent flows, a preliminary canonical test case is used to verify the fire spread component in Blaze in terms of rate of spread and computational cost. This is done in the A2F mode by simulating a simplified fire propagation over a flat terrain and forced by constant uniform wind simulated by MesoNH. This canonical case is detailed in Appendix B. Results show the good reproduction of the theoretical rate of spread due to Balbi and the good convergence of the fire front positions simulated by Blaze with respect to the fire mesh resolution Δx_f (changing from 25 m to 1 m) when using a RK3-WENO3 numerical scheme. The FireFlux [10] field-scale experiment is then used as a validation test case for Blaze when coupled with MesoNH in A2F,

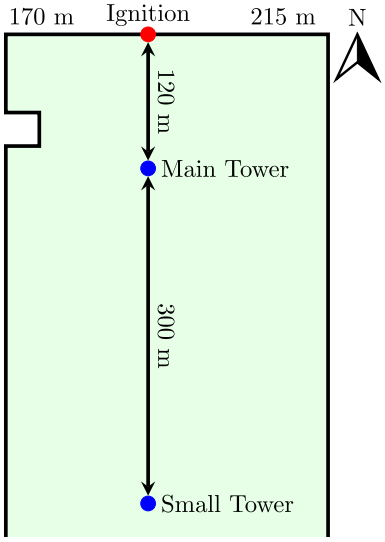

Fig. 3. Schematic of the FireFlux experimental field. The red dot represents the ignition point. The blue dots represent the main and small tower positions. The green area corresponds to the burn lot until the small tower. (For interpretation of the references to color in this figure legend, the reader is referred to the Web version of this article.)

F2A and 2WC modes.

4.2. FireFlux experiment

4.2.1. Experimental setup

The FireFlux experiment was conducted on 23 February 2006 at the Houston Coastal Center, a research center at the University of Houston, USA. It corresponds to a 30-ha fire burn (790 m by 385 m), where the main biomass fuel was tall grass. Fig. 3 presents an overview of the experimental field. The day before the burn, some of the biomass fuel properties were measured. The estimated dead fuel load (σ_d) was 1.04 kg m^{-2} [10], the dead fuel density (ρ_d) was 400 kg m^{-3}, the dead fuel moisture content (M_d) was 9%, and the fuel depth (e) was 1.5 m. The corresponding dead fuel packing ratio is $\beta_d = 1.7 \cdot 10^{-3}$. The live fuel represents 4% of the total fuel load [10] so that the live fuel load is $\sigma_l =$ 0.04 kg m^{-2} and the corresponding packing ratio is $6.7 \cdot 10^{-5}$. The live fuel moisture content M_l is about 200% [10].

The fire was ignited on the North side of the lot; the ignition process was carried out by two firefighters, who simultaneously light the western and eastern parts of the ignition line starting from the ignition point. The western line (respectively eastern) is 170 m long (respectively 215 m long), and is lit in 153 s (respectively in 163 s). The fire lasted about 15 min. Over the fire duration, the surface wind blew mainly from North to South with a limited magnitude (below 10 m s^{-1}) so that the fire propagated into the southern direction with a mean rate of spread of about 1.6 m s^{-1}. Measurements were recorded at two towers (blue dots in Fig. 3), the main tower and the small tower, which were 43 m high and 10 m high, respectively. The two towers were instrumented with sonic anemometers and regularly-spaced thermocouples. Turbulence and thermodynamic experimental measurements are reported in Refs. [8–10].

4.2.2. Simulation setup

To simulate the FireFlux experiment, the computational domain for MesoNH is 4 km by 7.5 km in the horizontal direction, and 1 km in the vertical direction. Ignition occurs at 12h43:30 LT (local time = UTC-5 h). The ignition point of the burn lot (red dot in Fig. 3) is located 500 m from the northern border and 2750 m from the western border of the domain. To be consistent with Filippi et al. [21], two different horizontal resolutions ($\Delta x = 10$ m referred to as A10, and $\Delta x = 25$ m referred to as A25 in the following) are tested. The grid is composed of 60 levels along the vertical direction. The grid is uniform with $\Delta z = 4$ m up to 45 m AGL. Above this height, the vertical grid resolution decreases with a geometrical progression; a ratio of 1.06 is imposed and leads to $\Delta z = 50$ m at an elevation of 1047 m AGL. A spin-up period, which corresponds to the interval between 12h00 LT and 12h43:30 LT, aims at obtaining an atmospheric state that is close to the actual meteorological conditions (the initial state of the atmosphere for this spin-up simulation is defined by the radiosonde launched at 06h55 LT). This spin-up time period was sufficient to match simulation to observations in terms of mean and variance statistics at the main tower.

In SURFEX, the ECOCLIMAP database is set to Atlantic coast grass. Table 4 gives the parametric values of the Balbi's rate-of-spread formulation used to simulate FireFlux. The residence time τ_f is assumed to be constant and is set to 17 s [1], which has implications on the fuel particle surface-area-to-volume ratio, $s_l = s_d = 4,446$ m^{-1}, since $\tau_0 = 75,590$ m^{-1} is a model constant [48] through the relation $\tau_f \equiv d/\mathcal{R} = \tau_0/s_d$ with d the front depth [51]. In the present study, the only difference between live grass fuel and dead grass fuel relates to the moisture content, since no other information on the live fuel is available for the FireFlux experiment.

The CST flux parameterization (Table 3) is used with the parameters given in Table 4 so that during the flaming residence time τ_f the latent heat flux is $\psi_w = 0.015$ kg m^{-2} s^{-1}, and the sensible heat flux is $\psi_h = 455$ kW m^{-1}. The values of these heat fluxes are also used to calibrate the EXS flux parameterization and have a similar energy release over the fire duration. The two parameters of the vertical flux distribution are set as $z_s = 5$ m and $z_{max} = 30$ m following numerical tests (not shown here).

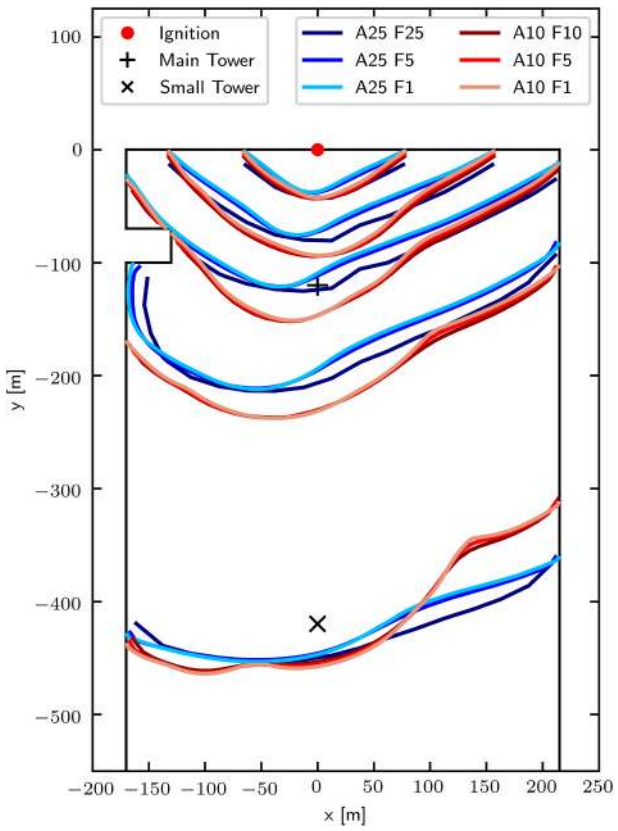

Fig. 4. FireFlux test case in forced mode (A2F) – Time-evolving fire front positions 1, 2, 3, 5, and 10 min after ignition (red dot) for 25-m (cool colors) and 10-m (warm colors) atmospheric forcing resolution (A25, A10) and several fire mesh resolutions (F25, F10, F5, F1). Black symbols represent the main tower (+) and small tower (x) positions. (For interpretation of the references to color in this figure legend, the reader is referred to the Web version of this article.)

Following some test results and Muñoz-Esparza et al. [36] recommendations, the RK3-WENO3 scheme is used in Blaze with the default values of 0.1 for artificial viscosity. The same spatial resolution is used in x- and y-directions (i.e. $\Delta x_f = \Delta y_f$).

To mimic the experimental ignition, drip torch ignition is used for both ignition lines in Blaze. The western 170-m long ignition line is lit in 153 s and the eastern 215-m long ignition line is lit in 163 s as in the experiment. Walking ignition is represented by imposing the arrival time at two points (x_a, y_a) and (x_b, y_b). Then, the points affected by the ignition between (x_a, y_a) and (x_b, y_b) are identified by Bresenham's line algorithm and by linearly interpolating the arrival time at these intermediate points. The value of the LS function φ at these points is computed by the time reconstruction approach described in Section 3.2. The thickness of the ignition line is thereby related to the fire mesh resolution Δx_f.

5. Results for the fireflux experiment

Several series of FireFlux simulation results in forced (A2F), fire replay (F2A) and two-way coupled (2WC) modes are presented in this section to provide insights into the MesoNH-Blaze coupling. The first objective is to determine the appropriate fire model resolution based on both spread and flux arguments (Section 5.1). The second objective is to highlight the sensitivity of the results to inflow turbulence (Section 5.2). The third and last objective is the validation of the coupled MesoNH-Blaze system by comparing coupled two-way simulation results with available measurements (Section 5.3).

5.1. Mesh convergence for fire spread and surface heat fluxes

The objective of the mesh convergence process is to determine the adequate fire mesh resolution for both spread and flux computations using one-way forcing modes (in forced mode A2F and in fire replay mode F2A).

5.1.1. Mesh convergence for fire spread in forced mode

Fig. 4 compares the time-evolving fire front positions for 25-m (A25 in cool colors) and 10-m (A10 in warm colors) atmospheric forcing resolution at 1, 2, 3, 5 and 10 min after ignition in forced mode (A2F). For each atmospheric forcing resolution, three different fire mesh resolutions are tested: fire refinement ratios of 1, 5 and 25 are used for the 25-m configuration, and ratios of 1, 2, and 10 are used for the 10-m configuration so that at the coarsest fire mesh resolution MesoNH and Blaze are run at the same resolution ($\Delta x_f = 25$ m for $\Delta x = 25$ m and $\Delta x_f = 10$ m for $\Delta x = 10$ m) and the most refined fire mesh resolution is $\Delta x_f = 1$ m in both cases. Each configuration is identified by its atmospheric resolution A and its fire resolution F. The simulation at 10-m atmospheric resolution with a fire mesh resolution of 5 m (*i.e.* refinement ratio of 2) is denoted by A10 F5.

Results in Fig. 4 show that all fire front positions are overlapped for the A10 atmospheric configuration, meaning that a 10-m fire mesh resolution is sufficient to obtain satisfactory fire spread simulations at 10-m atmospheric forcing resolution. For the A25 atmospheric configuration, the A25 F25 simulation gives a slightly different propagation from the A25 F5 and A25 F1 configurations due to a poorer description of the LS gradients and approximations in the burn plot geometry. Thus, a 5-m fire mesh resolution ensures a good fire front propagation for both A25 and A10 atmospheric configurations in A2F mode.

The fire arrival at the main tower (+ symbol in Fig. 4), around 3 min after ignition for A25 configuration and below 3 min for A10 configuration, is close to the observations (the observed arrival time is around 3 min after ignition) The early arrival for the 10 m configuration can be explained by the fact that Blaze does not account for the fire transient phase of its increasing power towards its steady state. In Blaze, as soon as the fire is ignited, it releases its nominal power and advances at a steady rate of spread. Ignoring this transient state then leads to an excessively fast propagation between the ignition point and the main tower in the simulations. This changes between the main tower and the small tower (x symbol in Fig. 4). There, the simulated fire spread is slower than in the observations (4 min to move from the main tower to the small tower in the observations against 7 min in the simulations). This could be explained by the lack of two-way atmosphere-fire coupling: injecting heat fluxes at the fire front may induce a local increase in horizontal wind and thereby in fire spread rate.

5.1.2. Mesh convergence for surface heat fluxes in fire replay mode

This section compares two methods for surface heat flux computation in terms of fire mesh convergence: the new EFFR method introduced in this study, and the WA method implemented in Blaze following what is implemented in WRF-SFIRE (Section 2.3.2).

The objective of the fire replay mode (F2A) is to study the MesoNH atmospheric response to the configuration of the surface heat flux forcing in Blaze (e.g. subgrid fire front reconstruction, heat flux parameterization). In the F2A mode, the fire replay is defined by a

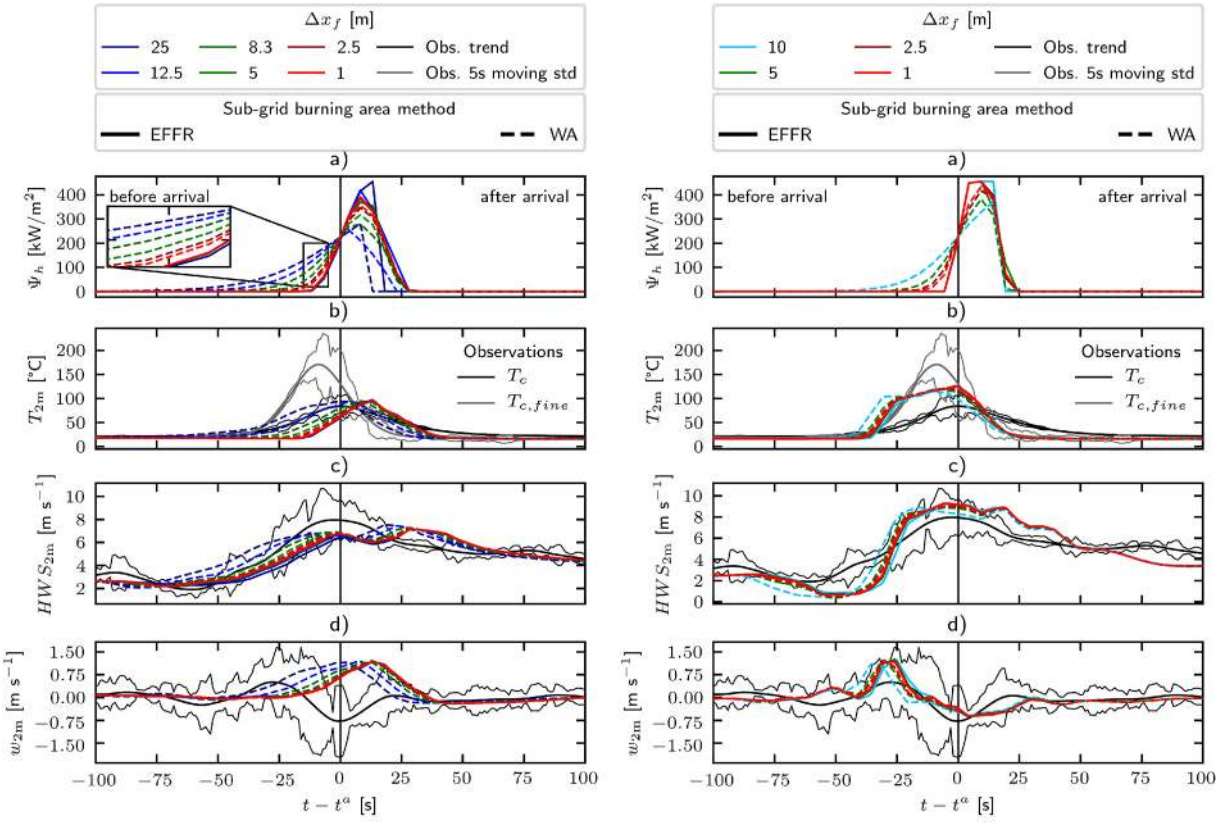

(a) A25 configuration (b) A10 configuration

Fig. 5. FireFlux test case in fire replay mode (F2A) – Time series of surface sensible heat flux, 2-m air temperature, 2-m horizontal wind speed and 2-m vertical wind speed at the main tower obtained for the CST flux parameterization. Colors represent different fire mesh resolutions (F25 to F1 in A25 configuration, F10 to F1 in A10 configuration). Solid lines correspond to EFFR results; dashed lines correspond to WA results. Black solid lines correspond to observations. (For interpretation of the references to color in this figure legend, the reader is referred to the Web version of this article.)

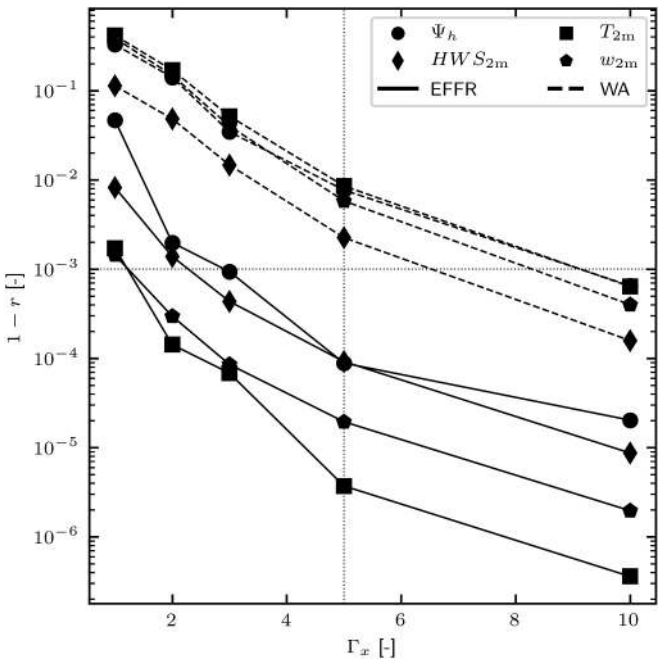

Fig. 6. FireFlux test case in fire replay mode (F2A) – Pearson correlation error with respect to the fire refinement ratio Γ_x for several atmospheric quantities simulated at the main tower for the A25 configuration: surface sensible heat flux (circles), 2-m air temperature (squares), 2-m horizontal wind speed (losanges) and 2-m vertical wind speed (pentagons). The error is computed with respect to the 1-m fire model results (fire refinement ratio equal to $\Gamma_x = 25$). Solid lines correspond to EFFR results; dashed lines correspond to WA results. The horizontal dotted line corresponds to the threshold $1 - r = 10^{-3}$.

burning map. In the present study, the burning map is obtained by taking the ensemble-mean burning map obtained in two-way coupled mode (2WC) with 10 m atmospheric resolution and 5 m fire resolution (configuration named A10 F5 in Section 5.3). The corresponding burning map is presented in Fig. 13. In this framework, a single atmospheric model simulation forced by the ensemble-mean A10 F5 burning map is run for two different atmospheric resolutions (A25 and A10). Fig. 5 shows the different atmospheric quantities obtained at the main tower for the A25 configuration (left column) and for the A10 configuration (right column), that is (from top to bottom panels) the sensible heat flux, the 2-m air temperature, the 2-m horizontal wind speed and the 2-m vertical wind speed.

The fire impact on the atmosphere at the main tower is clearly visible as a temperature peak, a horizontal wind acceleration and an updraft followed by a downdraft. Consider the A25 configuration in the left panel of Fig. 5. At 8.3-m resolution, the sensible heat flux computed by the EFFR method follows the 1-m resolution signal and convergence is achieved when resolution increases. The higher the resolution, the smoother the heat flux signal. Consistently, atmospheric variables are also converged for resolutions finer than 8.3 m. For the WA method, the heat flux profile is highly diffused ahead of the fire front for each considered resolution. The heat flux release begins too early, up to 70 s in advance of the fire arrival time for 25-m resolution and about 50 s in advance for 8.3-m resolution. This leads to an offset in the atmospheric variables, whereas the EFFR method already achieves a converged heat flux profile at the 8.3-m resolution. Hence, the EFFR method allows for a much faster convergence for the surface heat fluxes and the near-surface atmospheric variables than the WA method.

To go further, Fig. 6 represents the deviation from optimal Pearson correlation coefficient $r = 1$ with respect to the fire refinement ratio Γ_x for the EFFR and WA methods for different quantities of interest (surface sensible heat flux, 2-m air temperature, 2-m horizontal wind speed and 2-m vertical wind speed). This deviation measures for a given quantity of interest, the difference between a given fire mesh resolution and the 1-m fire mesh resolution considered as a reference. The closer this deviation is to 0, the more the signal is converged. Considering the criterion $r > 0.999$, i.e. $1 - r < 10^{-3}$ to achieve a good convergence on the A25 atmospheric variables, results show that a 8.3-m resolution is sufficient with the EFFR method, while a 2.5-m resolution is required with the WA method. The same trend is obtained for the A10 configuration.

The EFFR method can be used with a coarser resolution than the WA method to obtain similar results. For this purpose, a submetric fire model resolution is used in WRF-SFIRE (with the WA method) to simulate the FireFlux case [26,28,32]. The WA method requires a high computational effort for a result that is highly conditioned to the LS diffusion. In contrast, the EFFR method in MesoNH-Blaze gives a good heat flux profile even at 8.3-m fire model resolution. The heat flux signal is not as smooth as for higher resolutions. Hence, a 5-m fire model resolution appears as a good choice to ensure smooth heat flux injection and low computational effort for both A25 and A10 configurations.

Considering both spread arguments and flux arguments, the following MesoNH-Blaze results are obtained using the EFFR method for a fire mesh resolution equal to $\Delta x_f = \Delta y_f = 5$ m, i.e. for the A25 F5 and A10 F5 configurations.

5.2. Atmosphere and fire interactions in one-way mode

The objective of this section is to study some interaction effects between the atmosphere model and the fire model in one-way mode

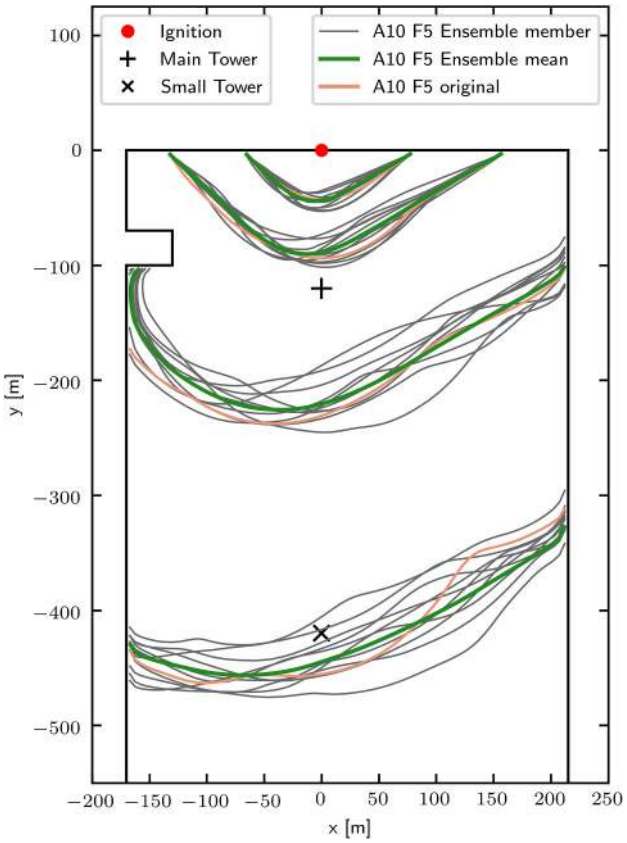

Fig. 7. FireFlux test case in forced mode (A2F) – Time-evolving fire front positions 1, 2, 5, and 10 min after ignition (red dot) for 10-m atmospheric forcing resolution (A10) and 5-m fire mesh resolution (F5) for a 15-member ensemble. Gray contours represent ensemble members. The green contour represents the ensemble mean. The orange contour represents the original A10 F5 front positions presented in Fig. 4. Black symbols represent the main tower (+) and small tower (x) positions. (For interpretation of the references to color in this figure legend, the reader is referred to the Web version of this article.)

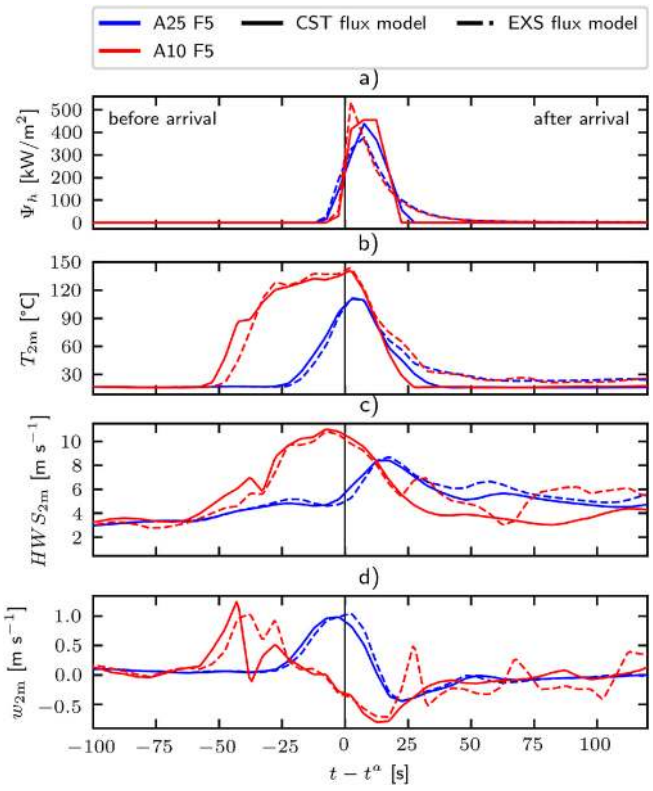

Fig. 8. FireFlux test case in fire replay mode (F2A) – Time series of (a) surface sensible heat flux, (b) 2-m air temperature, (c) 2-m horizontal wind speed, and (d) 2-m vertical wind speed at the small tower obtained for the CST (solid lines) and EXS (dashed-dotted lines) parameterizations in the A25 F5 (in blue) and A10 F5 (in red) configurations. (For interpretation of the references to color in this figure legend, the reader is referred to the Web version of this article.)

(forced mode A2F and fire replay mode F2A), that is *i)* the influence of atmospheric variability on the fire spread, and *ii)* the impact of the flux parameterization on the fire-induced flow.

5.2.1. Impact of the inflow turbulence variability on the fire spread in forced mode

Fig. 4 highlights that the simulated fire spread is different according to the atmospheric resolution. The initial state of the atmosphere is slightly different between the A25 and A10 configurations due to inflow turbulence, leading to a different local atmospheric forcing at the ignition time despite an average consistency. The arrival of different turbulent eddies then modifies the early propagation between the two configurations in a noticeable way. For instance, a larger northern wind anomaly in the A10 configuration accelerates the propagation shortly after ignition. Still, 10 min after ignition, the propagation is consistent between the two configurations despite a different shape. The fluctuation effects in the near-surface turbulent wind flow and their subsequent effects on the fire spread are considered using a statistical ensemble technique.

To account for the variability in the inflow turbulence, a 15-member ensemble of MesoNH-Blaze simulations was carried out for each atmospheric configuration in forced mode (A2F). To change the turbulent flow structure, the ensemble is generated by modifying the ignition time. Each member is ignited with a 2-min delay starting from 12h43 LT. Fig. 7 shows the resulting ensemble of front positions (gray colors) at 1, 2, 5 and 10 min after ignition for the A10 F5 configuration. The ensemble-mean (obtained by averaging ensemble burning maps) is plotted in green. The original A10 F5 simulation that was already presented in Fig. 4 and that was ignited at 12h43:30s LT does not belong to the ensemble and is plotted in orange for comparative purpose.

Results show that the incident turbulent structure has a significant impact on the fire spread with a difference in the fire front positions exceeding 80 m 10 min after ignition. Between the two towers, the fastest member gives a rate of spread 21% larger than the slowest member. A variability is also observed in the fire front curvature with various front shapes within the ensemble. This is also important since the fire front shape influences the wind projection on the fire front normal vector and thereby impacts the rate of spread. This highlights the importance to consider the inflow turbulence variability to assess the performance of a coupled atmosphere-fire model. An ensemble of simulations will be considered in two-way coupled mode (Section 5.3).

5.2.2. Impact of the surface heat flux parameterization on the atmosphere in fire replay mode

The sensitivity of the atmospheric variables to changes in the surface heat flux parameterization (CST or EXS, Section 2.3) in the fire replay mode (F2A) is now studied. Fig. 8 compares the atmospheric quantities of interest (from top to bottom panels: sensible heat flux, 2-m air temperature, 2-m horizontal wind speed, and 2-m vertical wind speed) simulated at the small tower for the A25 F5 configuration (blue curves) and for the A10 F5 configuration (red curves). By definition the CST (solid lines) and EXS (dashed-dotted lines) heat flux injection profiles mainly differ in their heat flux representation behind the fire front. That is why this study is done at the small tower, where the fire was ignited long enough to be able to preheat air flow behind the fire front and to be able to detect smoldering effects.

Fig. 8 shows that the heat flux injection profile is smoother for the EXS parameterization than for the CST parameterization with a smooth decay towards the smoldering zone (when $10 < t - t^a < 50$ s), as expected by their definition. The maximum heat flux intensity reached just after the fire arrival time (vertical solid line) is larger in the A10 configurations than in the A25 configurations due to change in the atmospheric resolution.

The effect of including smoldering in the EXS parameterization is particularly visible on the 2-m air temperature time series, where a heating from +5 °C to +11 °C can be observed in the smoldering area (when $t - t^a > 20$ s) for the EXS parameterization compared to the CST one.

On top of a temporal signature of the fire, Fig. 8 also provides a characterization of the spatial structure of the fire from right ($t - t^a > 0$ s, behind the fire front and upstream for the wind) to left ($t - t^a < 0$ s, ahead of the fire front and downstream for the wind). Upstream, there is a clear acceleration in the horizontal wind speed in the EXS configurations compared to the CST configurations. This effect is stronger at 10-m atmospheric resolution where the increase in horizontal wind speed can reach +3.1 m s^{-1}. This modifies the incident wind on the fire. This can be explained by the increase in temperature 20–25 s behind the fire front.

To go further, the instantaneous 2-m air temperature and horizontal wind fields for each configuration (A25 F5 CST and EXS in top panels, A10 F5 CST and EXS in bottom panels) are shown in Fig. 9. The smoldering zone that preheats the air behind the fire front is clearly visible. The flow structure is then significantly modified, especially for the A10 configurations, with a temperature along the front much more heterogeneous than for the CST parameterization. There are hot spots that seem more representative of an actual fire situation. The choice in the surface heat flux parameterization has therefore a significant impact on the fire-induced flow and will imply changes in the atmospheric feedback on the fire spread in 2WC mode. For this purpose, the EXS parameterization is used in the rest of the paper to account for smoldering.

5.3. Validation of MesoNH-Blaze model in two-way coupled (2WC) mode

In order to study the fire-atmosphere interactions, attention is now

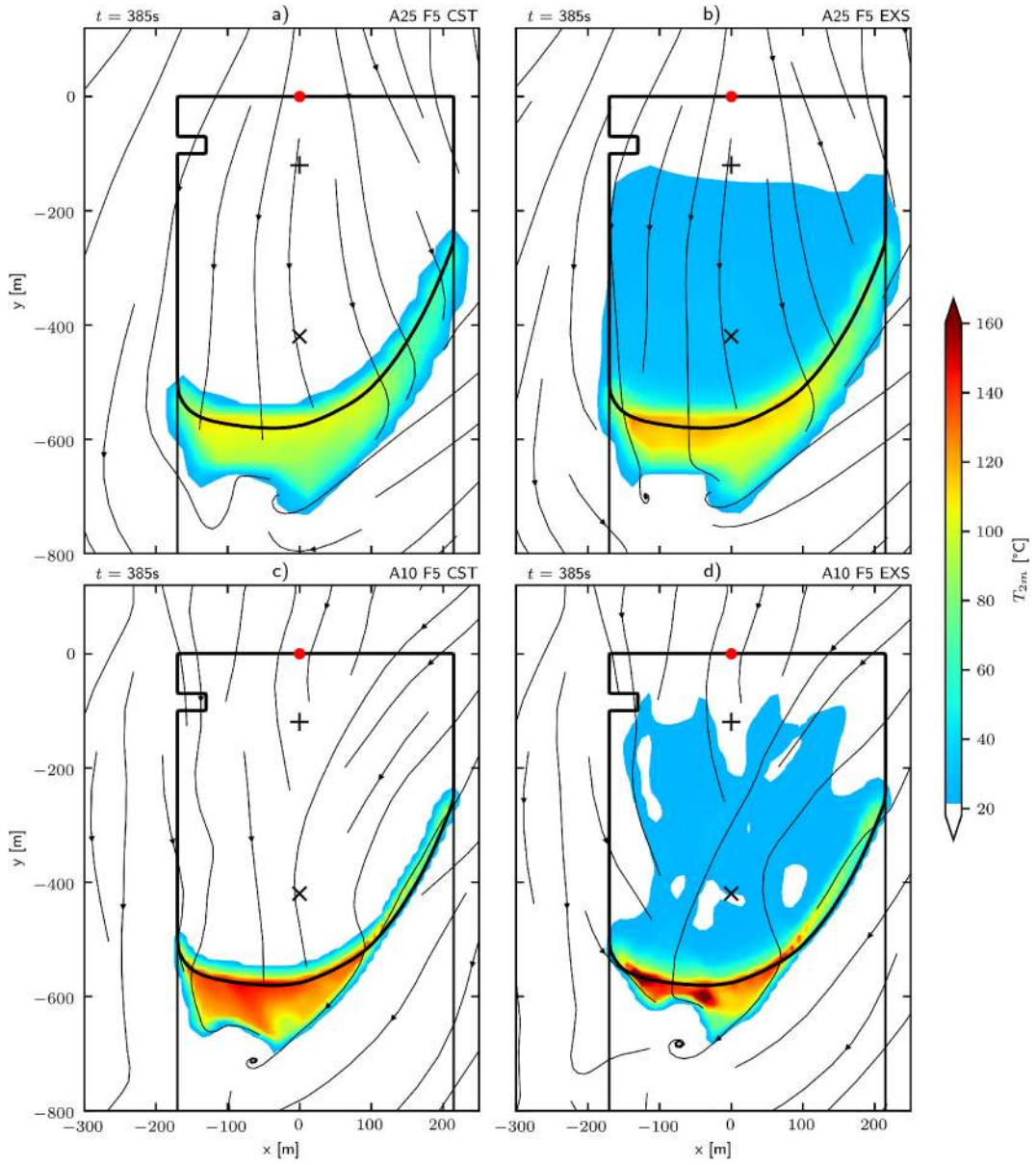

Fig. 9. FireFlux test case in fire replay mode (F2A) – Horizontal cross section at 2-m AGL for air temperature and horizontal wind fields in the following configurations: (a) A25 F5 and CST, (b) A25 F5 and EXS, (c) A10 F5 and CST, and (d) A10 F5 and EXS.

given to the two-way coupled mode that is able to represent the atmospheric feedback effects on the wildland fire behavior through the modification of the surface winds. Due to the significant impact of inflow turbulence on the fire spread shown in Section 5.2.1, a similar ensemble approach is adopted in 2WC mode. A 15-member ensemble is produced for each atmospheric resolution, A25 and A10, using the EXS flux parameterization. First, an analysis of the thermal plume is performed at the main tower. Second, the fire-induced flow is compared to the observations. Finally, the front propagation is evaluated in terms of spread rate and variability.

To compare simulations with measurements, a smoothing is performed using the Hodrick and Prescott [24] filter with a filtering constant of 1600 as recommended by the authors. It gives a smoother trend than the generally used 5-s averaging method [26,28]. The variability in the measurements is also represented by the 5-s standard deviation. The measurements are positioned on the time axis by considering the correlation between the arrival time and the temperature peak on the time series. For measurements, the Type T thermocouple is considered to be a better quality measurement and the time calibration is fixed on this signal. There is a significant variability difference between the measurements of the two thermocouples at the main tower. This is due to the shorter response time of the Type K thermocouple compared to its Type T counterpart.

5.3.1. *Thermal plume*

Fig. 10 shows the time series of air temperature at all heights of the main tower (2 m, 10 m, 28 m and 42 m) for the A25 F5 and A10 F5 ensembles along with the *in situ* measurements. The ensemble mean is represented by the solid line, and the turbulence variability is accounted by the standard deviation of the ensemble in colored area (blue for A25 and red for A10). Results show that the temperature increase due to the fire passage is well represented by the coupled model. The temperature peak is reached at all heights with a slight delay, in particular at 10 m resolution, meaning that the plume is too vertical compared to the measurements. At 2 m height, the simulation temperature results are of the same order of magnitude as the two sets of observations. Above 2 m, the A10 ensemble is closer to the observed amplitude. The variability resulting from the inflow turbulence increases with altitude. This

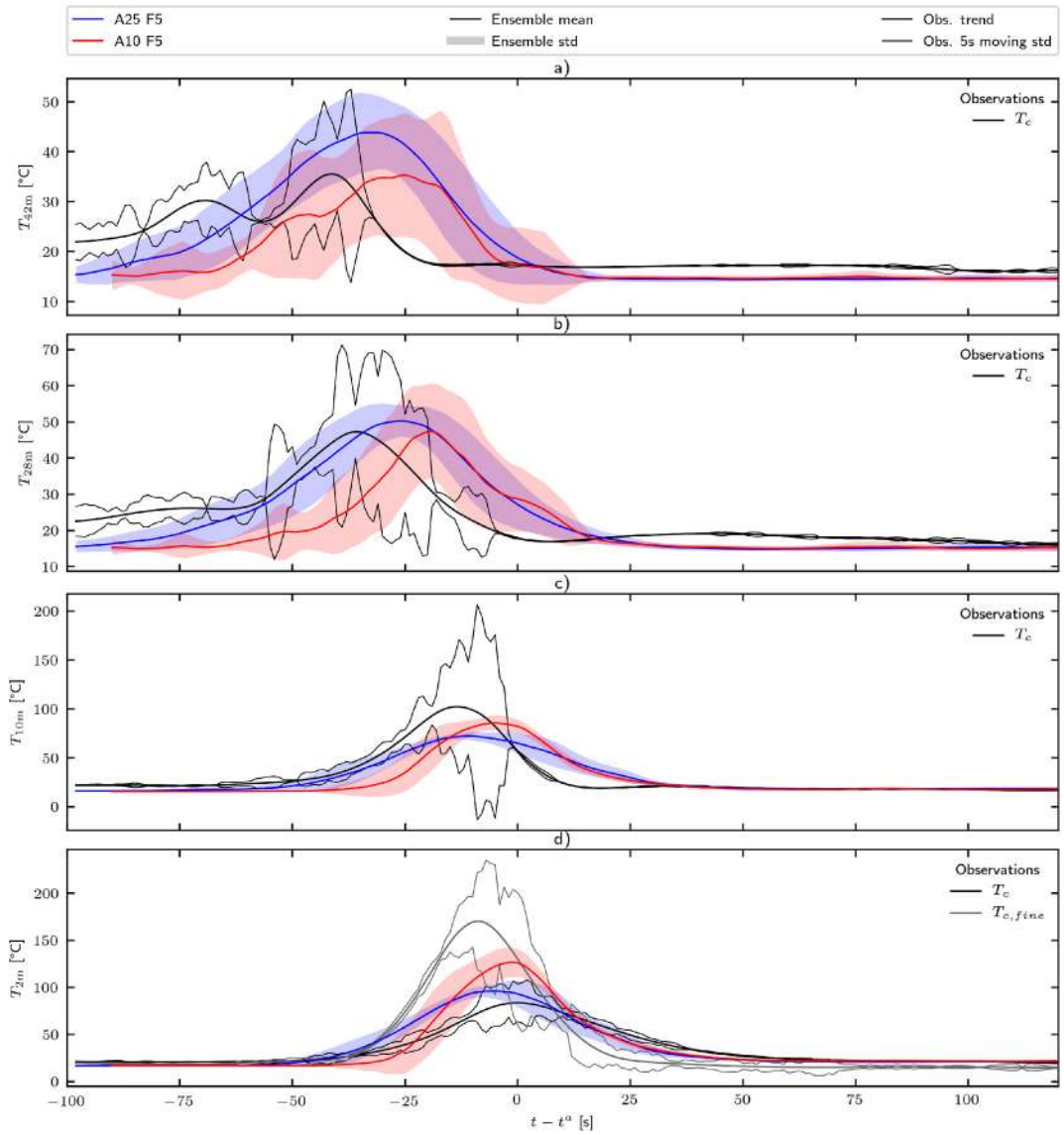

Fig. 10. FireFlux test case in two-way coupled mode (2WC) – Temporal evolution at the main tower of air temperature at different heights: (a) 42 m, (b) 28 m, (c) 10 m, and (d) 2 m, for A25 F5 (blue colors) and A10 F5 (red colors) ensembles. Available measurements are given in gray and black colors. (For interpretation of the references to color in this figure legend, the reader is referred to the Web version of this article.)

variability is particularly important at the temperature peak but also at the time of plume passage. Some members of the ensemble can therefore give a thermal plume structure closer to the measurements than the ensemble mean, highlighting again the importance of running an ensemble for coupled atmosphere-fire models.

5.3.2. *Fire-induced wind*

Fig. 11 shows the horizontal wind induced by the fire passage at the main tower. The wind acceleration at 2 m and 10 m height (Fig. 11d) is well captured by the coupled model for both A10 F5 and A25 F5 configurations despite the sensor fail at 10 m AGL. Above 10 m, the wind is slower in the simulations than in the measurements. This could explain why the thermal plume is too vertical. The ensemble variability is slightly more important in the A10 configuration than in the A25 configuration.

Fig. 12 shows the vertical wind induced by the fire passage at the main tower. The updraft/downdraft alternation is fairly well represented, despite the significant time lag from a slightly different plume inclination than the one observed. The coupled model gives higher values of updraft velocity compared to measurements, which reinforces the vertical orientation of the simulated plume. Again, the variability due to inflow turbulence increases with altitude and is more important at 10 m resolution. This indicates that MesoNH-Blaze at high resolution is more sensitive to the inflow turbulence conditions for the scale of the FireFlux experiment, which remains of limited size compared to active wildfires.

Overall, the thermal structure of the plume and the fire-induced wind are reasonably well represented by the MesoNH-Blaze coupled model.

5.3.3. *Fire spread*

Fig. 13 compares the fire front positions at different times for the A25 F5 and A10 F5 ensembles. The A10 F5 ensemble obtained in forced mode (A2F) is also represented to highlight the significant influence of the atmospheric feedback on the fire behavior. Results show large discrepancies in the fire front propagation between the 2WC simulations (blue curves for A25 F5 and red curves for A10 F5), and the A2F simulations (green curves). Accounting for the wind acceleration induced at the front by the fire energy release enhances fire propagation in 2WC mode. This also provides more curved fronts, which seem more realistic of actual fire propagation than in the forced mode. Results also show

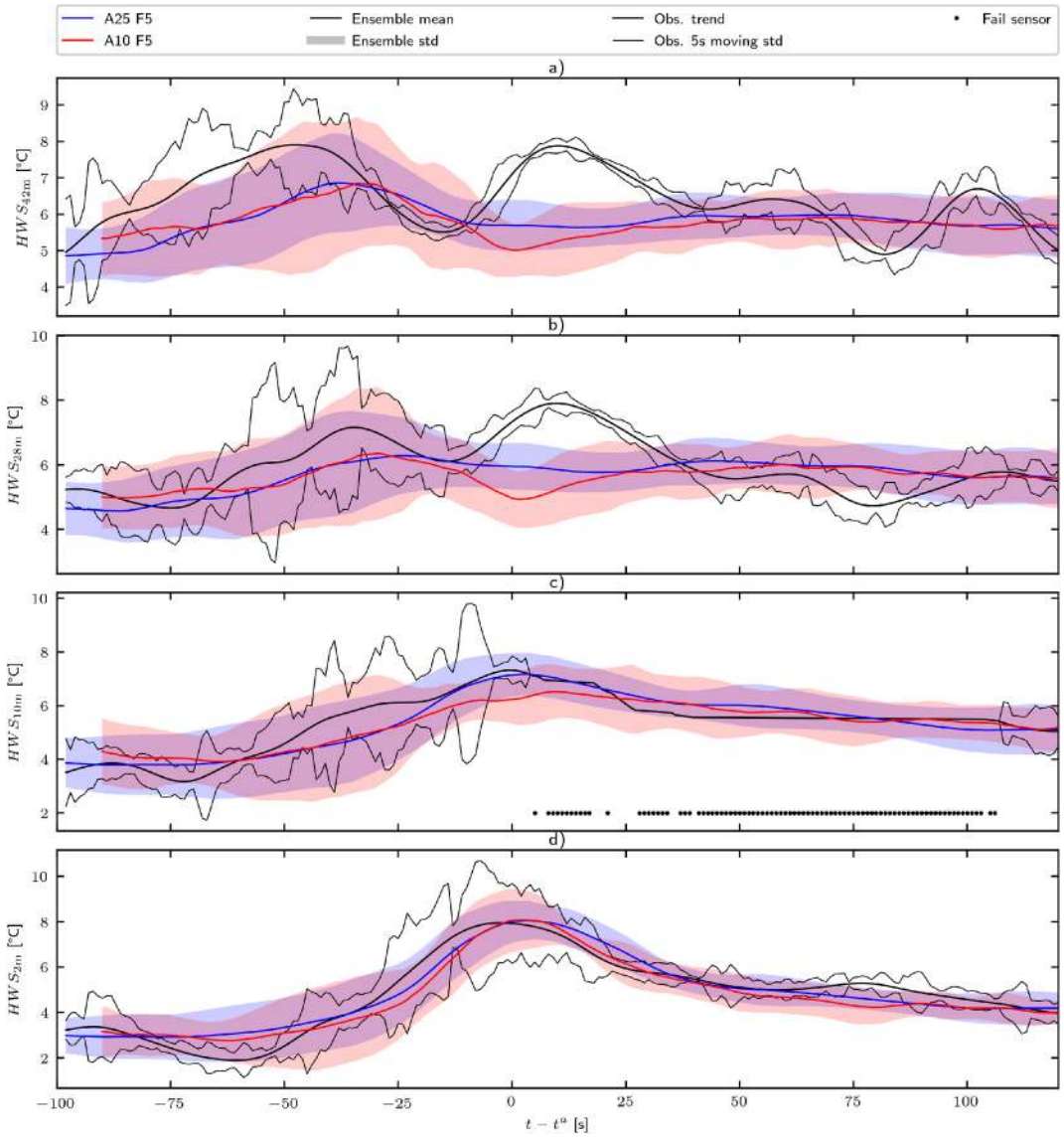

Fig. 11. FireFlux test case in two-way coupled mode (2WC) – Temporal evolution at the main tower of horizontal wind speed (HWS) at different heights: (a) 42 m, (b) 28 m, (c) 10 m and (d) 2 m, for A25 F5 (blue colors) and A10 F5 (red colors) ensembles. Available measurements are given in gray and black colors. (For interpretation of the references to color in this figure legend, the reader is referred to the Web version of this article.)

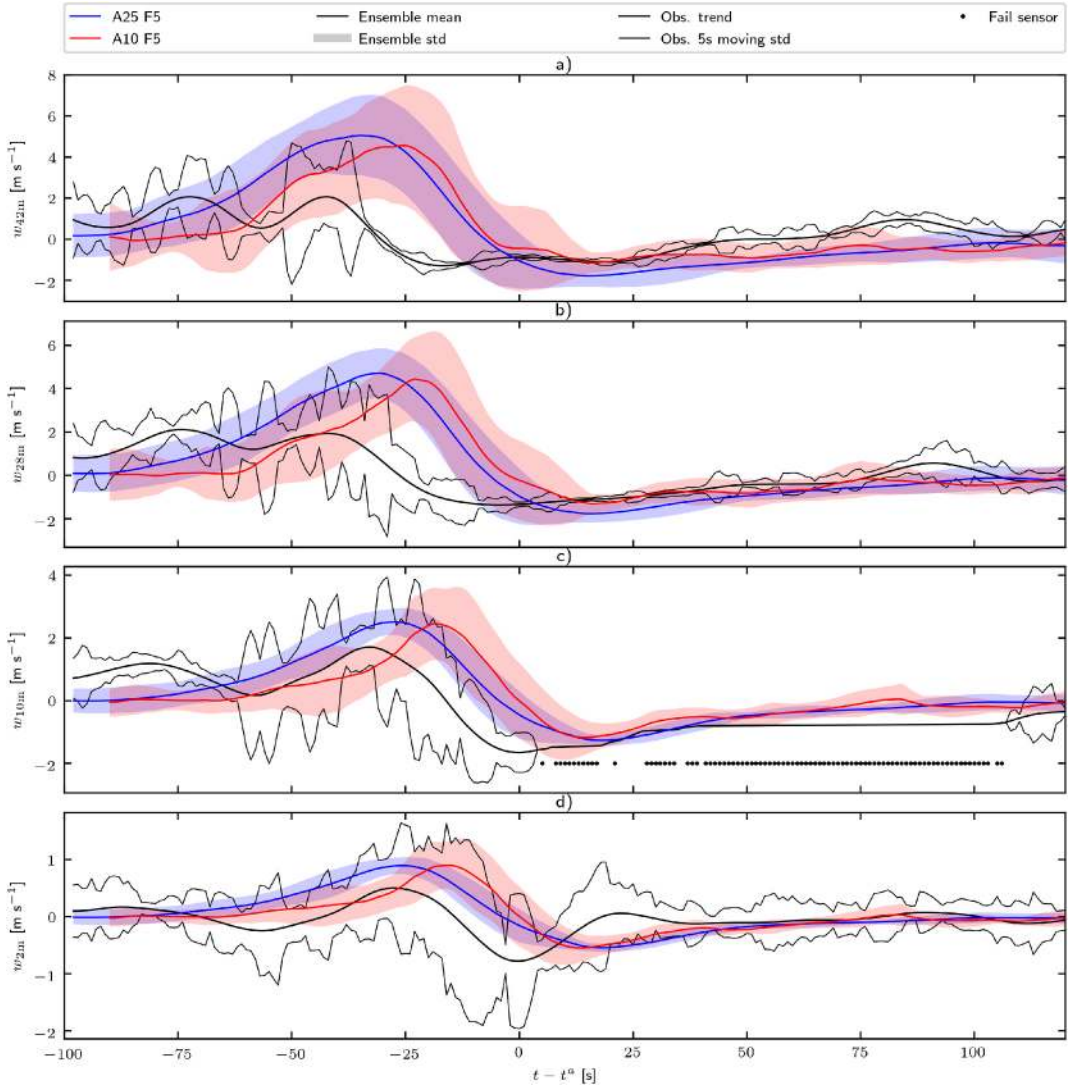

Fig. 12. FireFlux test case in two-way coupled mode (2WC) – Temporal evolution at the main tower of vertical wind speed at different heights: (a) 42 m, (b) 28 m, (c) 10 m and (d) 2 m, for A25 F5 (blue colors) and A10 F5 (red colors) ensembles. Available measurements are given in gray and black colors. (For interpretation of the references to color in this figure legend, the reader is referred to the Web version of this article.)

that the variability in the fire front positions is enhanced in the 2WC mode compared to the A2F mode, meaning that inflow turbulence has a stronger impact on the fire behavior in two-way mode than in forced mode.

For the FireFlux experiment, the only way to evaluate the fire spread simulated by the MesoNH-Blaze coupled model is through the time-averaged rate of spread between the main and small towers since this is the only measurement of the actual rate of spread. Rate-of-spread statistics are given in Table 5. The observed rate of spread was 1.61 m s^{-1}. In the ensemble simulations, the ensemble-averaged rate of spread (denoted by $\bar{\mathcal{R}}\left(t_k^a\right)$) is estimated as follows: the averaged rate of spread between the two towers is first computed for each ensemble member, and is then averaged over the ensemble. Additional statistics such as the minimum/maximum interval and the standard deviation are also given. Looking at the ensemble-averaged rate of spread, relative errors are −2.5%, −0.6%, and −53% for the 2WC A25 F5, 2WC A10 F5 and A2F A10 F5, respectively.

The actual coupled model configuration thereby provides a good estimate of the time-averaged rate of spread between the two towers. The contribution of the coupling is significant since the proper representation of the horizontal wind induced by the fire leads to an increase in the spread rate to match the observed value. The variability due to inflow turbulence is higher in two-way coupled mode than in forced mode, especially at 10-m atmospheric resolution where one member is much slower than the others (1.25 m s^{-1}, i.e. 22% slower than the ensemble average). This variability is not evenly distributed along the fire front. It is mostly concentrated on the eastern flank, where a small deviation of the wind direction induces a large variation of the wind projection on the normal direction of the front and thereby on the spread rate.

6. Discussion

In order to better represent the fire-induced wind and fit the observed mean rate of spread between the two instrumented towers in

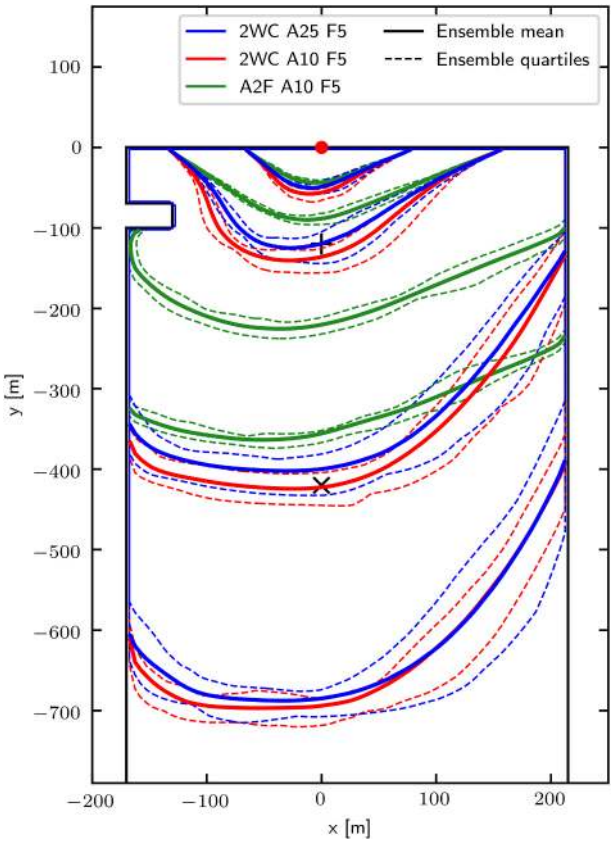

Fig. 13. FireFlux test case in two-way coupled mode (2WC) – Time-evolving fire front positions at 1, 2, 5, and 8 min after ignition (red dot) for A25 F5 and A10 F5 ensembles. The A2F ensemble obtained for the A10 F5 configuration is also plotted for comparative purpose. Solid lines represent the ensemble mean. Dashed lines represent the quartiles. Black symbols represent the main tower (+) and small tower (x) positions. (For interpretation of the references to color in this figure legend, the reader is referred to the Web version of this article.)

the coupled simulations, a simple parameter adjustment has been performed on the ignition temperature T_i involved in Balbi's parameterization. T_i is known to be one of the predominant factors to which the simulated rate of spread is sensitive. The combustion efficiency E_c has also been calibrated to obtain realistic heat fluxes. This two-parameter adjustement has been successful to obtain realistic simulations of the atmosphere-fire interactions, providing a first validation of the new MesoNH-Blaze coupled model on the FireFlux I experimental fire.

Considering the air preheating in the burnt region, the smoldering area behind the fire front has an effect on the flow in the vicinity of the fire front and thereby significantly influences the fire spread. The flux parameterization and its impact at different scales would deserve further investigation in future work.

The reconstruction of the LS function from the burning map takes advantage of the bounded formulation $0 \leqslant \varphi \leqslant 1$, but requires the calibration of the stiffness parameter λ. In this study, λ is considered as a function of the fire mesh size Δx_f only. The formulation of λ has been adjusted on a simplified fire experiment and with a given fuel type. It would be more exhaustive to consider λ as a function of at least the fire mesh size Δx_f, the rate of spread without wind $\mathcal{R}_0$ (which is exclusively related to the biomass fuel) and the wind contribution to the rate of spread $(\mathcal{R} - \mathcal{R}_0)$ (which differentiates the head fire and the back fire). This would allow a more accurate reconstruction in forced mode (F2A) runs and be more adapted for walking ignition.

Table 5
Rate-of-spread statistics obtained between the main and small towers for 2WC ensembles at 25-m and 10-m atmospheric resolutions and for A2F ensemble at 10-m atmospheric resolution. The observed rate of spread is also given for comparative purpose.

Configuration	2WC A25 F5	2WC A10 F5	A2F A10 F5	Observations
$\min_k \mathcal{R}(t_k^a)$	1.44	1.25	0.67	
$\bar{\mathcal{R}}(t_k^a)$	1.57	1.60	0.75	1.61
$\max_k \mathcal{R}(t_k^a)$	1.68	1.75	0.81	
$\mathrm{std}_k \mathcal{R}(t_k^a)$	0.08	0.11	0.04	

The EFFR method is useful to have a less refined fire mesh in the coupled atmosphere-fire model compared to the WA method, for instance employed in WRF-SFIRE. At 10-m atmospheric resolution, Blaze can operate at 5-m resolution and provide relevant results without the need to go to submetric resolution as done in some WRF-SFIRE studies. For 2WC simulations, the relative additional computational cost associated with the fire model is 8% for the EFFR method against 25% for the WA method. At 25-m atmospheric resolution, the relative additional computational cost associated with the EFFR method is 14%. The EFFR method is thereby useful to save computational time in MesoNH-Blaze, in particular when running ensembles of simulations to account for inflow turbulence.

7. Concluding remarks

This paper presents an implementation of an innovative level-set formulation in the scope of the Blaze fire model coupled with an atmospheric model to be able to run ensembles of coupled atmosphere-fire simulations in an effective way. The FireFlux I field-scale experimental fire is used to evaluate Blaze when coupled with the MesoNH atmospheric model using one-way or two-way coupling modes. High-order schemes (RK3, WENO3) have been integrated in Blaze to ensure accurate propagation at a reasonable computational cost. These numerical schemes provide a very low rate-of-spread error (less than 0.1%) on a uniform wind case without the need to reinitialize the level set. Numerical viscosity is applied to the level-set function as in Mandel et al. [32]and is also applied to the rate of spread to smooth out local variations due to inflow turbulence. Results show that under turbulent flow, Blaze features very good mesh convergence in forced mode (A2F) and fire replay mode (F2A), and that a 5-m fire mesh resolution provides a satisfactory solution for the FireFlux case that corresponds to a homogeneous grass fuel. This was possible thanks to the explicit fire front reconstruction (EFFR) method, which better localizes the heat fluxes and thereby improves the coupling of Blaze with the atmosphere model. The EFFR method was compared to the weighted average (WA) method, for instance employed in WRF-SFIRE [28,32,36]. Results show that the EFFR method outperforms the WA method in terms of mesh convergence, meaning that a much coarser fire model resolution can be used for equivalent performance using the EFFR method (5 m for EFFR compared to 1 m for WA). This economy in mesh refinement translates into improved code efficiency and consequently reduced computational cost for similar performance of MesoNH-Blaze. Sensitivity tests were carried out to analyze the response of coupled atmosphere-fire simulations to changes in the surface heat fluxes and inflow turbulence. Sensitivity results show that accounting for smoldering through the EXS

parameterization induces a noticeable change in the structure of the incident flow in the vicinity of the fire. The incident wind accelerates and hot spots are present along the fire front. Sensitivity results also show the significant impact of the inflow turbulence on the fire front propagation. In A2F mode, the rate of spread can differ by up to 21% between the ensemble members. A detailed study in forced fire-to-atmosphere (F2A) mode and two-way coupled (2WC) mode demonstrated the good correlation between FireFlux I measurements and ensemble simulations at 25-m and 10-m atmospheric resolution in the range of variability of the measurements. The variability due to the incident turbulent structure remains however very large, with stronger effects in altitude and at finer atmospheric resolution. Some members in the ensemble were found to be very close to measurements due to favourable inflow turbulence. This implies that a good agreement between a single member and the measurements does not necessarily reveal a good agreement between the model and the reality since the signal at the tower is strongly conditioned by the inflow turbulence. The present study thereby highlights the importance of accounting for the variability of the near-surface wind flow at the scale of an experimental fire such as FireFlux I. The FireFlux I experiment is a first validation test case for the newly-implemented MesoNH-Blaze coupled model. Terrain is flat, wind conditions are moderate, and biomass fuel is homogeneous and corresponds to grass. Future work includes extending the validation of MesoNH-Blaze to cases of increasing complexity, starting from different types of biomass fuels, including forest environment, to study the coupled model response to combined effects of inflow turbulence, canopy turbulence and fuel variability. This is an important step to validate the ability of MesoNH-Blaze to simulate realistic wildland fire behavior for different biomass fuels and different landscapes.

CRediT authorship contribution statement

Aurélien Costes: Conceptualization, Methodology, Software, Validation, Writing - Original draft preparation. **Mélanie C. Rochoux:** Supervision, Writing - Review & Editing, Project administration, Funding acquisition. **Christine Lac:** Supervision, Writing - Review & Editing, Project administration, Funding acquisition. **Valéry Masson:** Supervision, Writing - Review & Editing.

Declaration of competing interest

The authors declare that they have no known competing financial interests or personal relationships that could have appeared to influence the work reported in this paper.

Acknowledgements

The Authors gratefully acknowledge support from ANR (ANR-16-CE04-0006, FIRECASTER) and LEFE/INSU. The Authors gratefully acknowledge Jean-Baptiste Filippi (CNRS) and Ronan Paugam (Cerfacs) for helpful discussions on coupled atmosphere-fire modeling and wildland fire modeling. They also acknowledge Juan Escobar (LA) for support on MesoNH.

Appendix A. Supplementary data

Supplementary data to this article can be found online at https://doi.org/10.1016/j.firesaf.2021.103475.

Appendices A. Balbi's rate-of-spread parameterization

This Appendix provides all the equations required to estimate the rate of spread $\mathcal{R}$ from Balbi's formulation given the definition of the input parameters in Table 4. These equations are taken from Santoni et al. [48].

A.1 Notations

A mix of live and dead vegetation is considered to represent the biomass fuel; the subscripts "l" and "d" are, respectively, for 1-h dead and thin live fuels in the following. The packing ratios, denoted by β_l and β_d, are computed for both live and dead fuels as

$$\beta_l = \frac{\sigma_l}{e\rho_l}, \quad \beta_d = \frac{\sigma_d}{e\rho_d}, \tag{A.1}$$

where e [m] is the fuel layer thickness, σ_l [kg m^{-2}] (σ_d) is the live (dead) fuel surface loading, and ρ_l [kg m^{-3}] (ρ_d) is the live (dead) fuel particle mass density. For clarity purposes, we introduce the following notations:

$$S_l = s_l\, e\, \beta_l = \frac{s_l\, \sigma_l}{\rho_l}, \quad S_d = s_d e \beta_d = \frac{s_d\, \sigma_d}{\rho_d}. \tag{A.2}$$

A.2 Nominal radiant temperature

We introduce the dimensionless variable ξ as

$$\xi = \frac{(M_l - M_d)\, S_l\, \Delta h}{S_d\, \Delta H}, \tag{A.3}$$

where Δh [MJ kg^{-1}] is the water evaporation enthalpy and ΔH [MJ kg^{-1}] is the combustion enthalpy. The nominal radiant temperature denoted by T_n is then estimated as

$$T_n = T_a + \frac{\Delta H\,(1-\chi_0)\,(1-\xi)}{c_{pa}\,(1+s_t)}, \tag{A.4}$$

where T_a [K] is the air temperature, c_{pa} [J K^{-1} kg^{-1}] is the air calorific capacity, χ_0 [-] is the radiant heat transfer fraction and s_t [−] is the air/fuel stochiometry ratio.

A.3 Flame tilt angle

The flame gas velocity v_0 [m s^{-1}] satisfies

$$v_0 = \nu\,\frac{2\,LAI\,(1+s_t)\,T_n\,\rho_d}{\rho_a\,T_a\,\tau_0}, \tag{A.5}$$

where LAI is the leaf area index, and ν [−] is the absorption coefficient for radiation defined as

$$\nu = \min\left(\frac{S_d}{LAI}, 1.\right) \tag{A.6}$$

Then, the flame tilt angle γ [rad] is defined as

$$\tan\left(\gamma\right) = \tan\left(\alpha_{sl}\right) + \frac{U}{v_0}, \tag{A.7}$$

where α_{sl} [rad] is the slope angle, and U is the horizontal wind speed at mid-flame height in the spread direction. In Balbi's rate-of-spread formulation, the wind is given in the fire front propagation direction.

A.4 No-wind no-slope rate of spread

By defining

$$a = \frac{\Delta h}{c_p(T_i - T_a)}, \tag{A.8}$$

$$R_{00} = \frac{B\,T_n^4}{c_p\,(T_i - T_a)}, \tag{A.9}$$

where c_p [J K^{-1} kg^{-1}] is the fuel calorific ratio, T_i [K] is the ignition temperature, and $B = 5.670373 \times 10^{-8}$ [W^{-2}m K^{-4}] is the Stefan-Boltzmann constant, the rate of spread without wind and slope, denoted by $\mathcal{R}_0$ [m s^{-1}], is estimated as

$$\mathcal{R}_0 = \frac{e\,R_{00}}{\sigma_d\,(1+a\,M_d)}\left(\frac{S_d}{S_d+S_l}\right)^2. \tag{A.10}$$

Hence, $\mathcal{R} = \mathcal{R}_0$ if the flame tilt angle is such as $\gamma \leqslant 0$.

A.5 Wind- and slope-aided rate of spread

For a flame tilt angle $\gamma > 0$, we define the following quantities:

$$A_0 = \frac{\chi_0\,\Delta H}{4\,c_p\,(T_i - T_a)}, \tag{A.11}$$

$$A = \frac{\nu\,A_0\,(1-\xi)}{1+a\,M_d}, \tag{A.12}$$

$$r_0 = s_d\,r_{00}, \tag{A.13}$$

$$G = \frac{r_0(1 + \sin\gamma - \cos\gamma)}{\cos\gamma}, \tag{A.14}$$

$$\mathcal{R}_t = \mathcal{R}_0 + AG - \frac{r_0}{\cos\gamma}, \tag{A.15}$$

where r_{00} [m s^{-1}] is the radiant heat transfer parameter. The wind-/slope-aided rate of spread $\mathcal{R}$ is finally given by

$$\mathcal{R} = \frac{1}{2}\left(\mathcal{R}_t + \sqrt{\mathcal{R}_t^2 + \frac{4\, r_0\, \mathcal{R}_0}{\cos\gamma}}\right) \tag{A.16}$$

B Verification test case for Blaze: fire spread with uniform wind

This Appendix presents a test case to verify the good numerical behavior of the spread component in the Blaze fire model in the A2F mode (Fig. 2a). The objective is to show that the simulated rate of spread corresponds to the theoretical values given by Balbi's parameterization (Appendix A) along the fire front without considering the coupling with the atmosphere. The verification test case corresponds to a simplified fire propagation over a flat terrain with weak uniform wind (no turbulence is considered) and with a single ignition spot.

B.1 Numerical settings

The 3-D computational domain is 3.6-km by 2-km by 244 m. In MesoNH, the horizontal resolution is 25 m and the vertical direction is discretized with 40 vertical levels: the first level is at 4-m; a stretching ratio of 1.02 is applied until 200-m AGL and above this ratio becomes 1.05. A constant wind is set at the west border of the domain varying along the vertical from 2.3 m s^{-1} at the ground to 6.5 m s^{-1} above 100 m AGL. Lateral boundary conditions are cyclic. The reference pressure is 1017.10 hPa. The ground air temperature is 286 K. The land surface (e.g. roughness length, vegetation classes, land/water mask, soil texture) is described with the SURFEX platform [34]. In Blaze, the same biomass fuel as for the FireFlux experiment is used (Table 4), leading to a no-wind no slope rate of spread $\mathcal{R}_0 = 0.5\,\mathrm{m\,s^{-1}}$ and a mean wind-aided rate of spread $\bar{\mathcal{R}} = 0.9\ \mathrm{m\,s^{-1}}$. The ignition spot is a 50-m side squared patch that is 1225 m away from the western boundary and 1000 m away from the southern boundary.

The same numerical schemes as for the FireFlux experiment are used: RK3-WENO3 for advection combined with PPM for scalar tracer advection in MesoNH; RK3-WENO3 in Blaze but no artificial viscosity is added since there is no turbulence in the present test case.

Blaze is run for several fire mesh resolutions (Δx_f, Δy_f) to verify the convergence of the fire spread component. The same fire resolution is used along the x- and y-axis ($\Delta x_f = \Delta y_f$). Six fire refinement ratios Γ_x (1, 2, 3, 5, 10, and 25) are tested so that the fire mesh size Δx_f varies between 25 m and 1 m for the different Blaze configurations.

B.2 Results and discussion

Fig. 14a compares the fire front positions at 5-min time intervals for the six different fire refinement ratios. Results for a fire refinement ratio equal to 1 are indicated in blue line (this corresponds to the same resolution between MesoNH and Blaze); results for a fire refinement ratio equal to 25 are indicated in red line (this corresponds to the finest resolution tested in Blaze). The theoretical fire front position obtained using the standalone Balbi's parameterization are indicated in black lines at the head fire, on the flanks and at the back fire. Fig. 14b shows the evolution of the rate-of-spread relative error as the fire refinement ratio Γ_x increases, i.e. as the fire mesh resolution increases. This error is computed with respect to Balbi's theoretical rate of spread.

Results show that the fire spread is symmetrical with respect to the y-axis as expected under uniform wind conditions blowing from the West. Each fire mesh resolution, from 25 m to 1 m, is able to correctly propagate the fire over the 20-min time period. The choice of the fire mesh resolution has some slight impact in high curvature areas. Blaze is able to match the theoretical rate of spread given by Balbi's parameterization. At the head fire and the back fire, the rate-of-spread error is dropping exponentially with the fire mesh refinement. The rate-of-spread error is about 0.16% for $\Delta x_f = 25$ m and -0.01% for $\Delta x_f = 1$ m.

It is of high interest to compare the head rate-of-spread error rates with those obtained in Muñoz-Esparza et al. [36]. In Ref. [36], when using the RK3-WENO3 numerical scheme, the rate-of-spread error is respectively -10% and -7% for 25-m and 12.5-m fire mesh resolutions. It increases to -15% and -10% when using the ENO1-RK2 scheme implemented in SFIRE [32]. In Blaze, at 12.5-m resolution (i.e. refinement ratio $\Gamma_x = 2$), the rate-of-spread error is equal to 0.1% when using RK3-WENO3 without adding numerical viscosity. To reduce the error magnitude to 0.1%, Muñoz-Esparza et al. [36] shows that the fire spread model requires a higher order numerical scheme (WENO5) and reinitializing the LS function, which significantly increases the computational cost (by about 30%).

To conclude, Blaze provides a good balance in terms of rate-of-spread error and computational cost to be coupled with an atmosphere model for simulating experimental fires such as the FireFlux experiment. Such numerical studies will have to be revisited for large-scale wildfires, which are subject to heterogeneous fuel properties and spatially-varying winds enhanced by terrain topography.

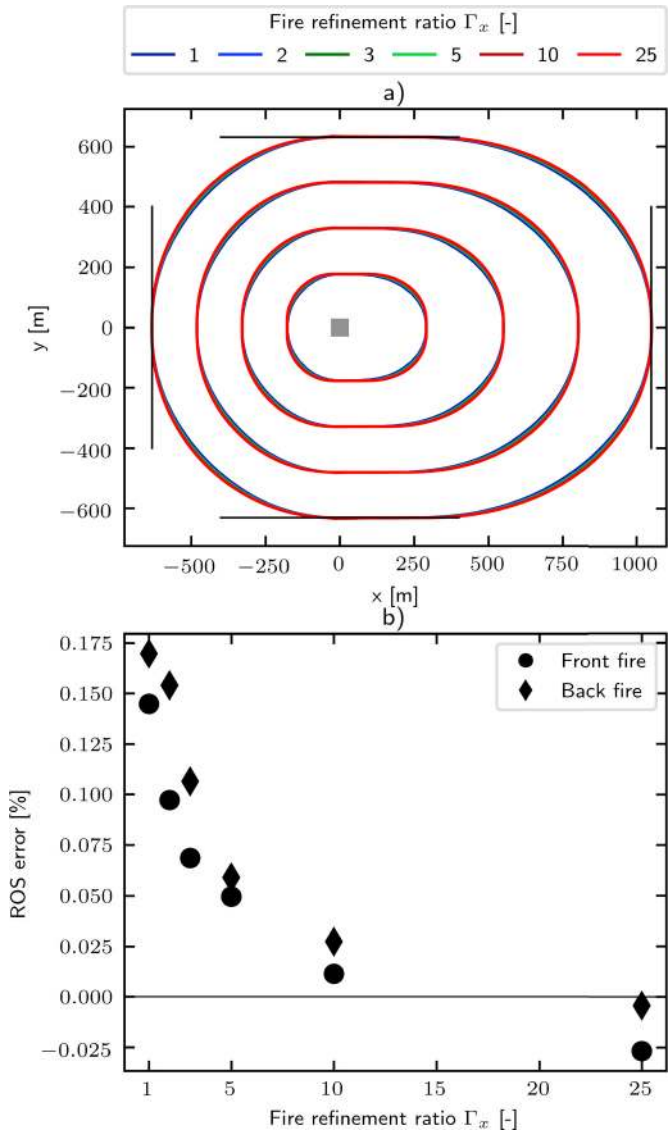

Fig. 14. Results for the verification test case with uniform wind and single ignition point (gray box). (a) Time-evolving fire front positions over a 20-min time period: the fire fronts are plotted at 5-min time intervals for each fire refinement ratio Γ_x (one color corresponds to one fire refinement ratio). The black lines correspond to the fire front position at time 20 min if the fire spread model was perfectly integrated without numerical errors. (b) Relative rate-of-spread error [%] at time 20 min at the head fire (circle symbols) and at the back fire (diamond symbols).

References

[1] H.E. Anderson, Heat Transfer and Fire Spread, USDA Forest Service Research Paper INT, 1969, 10.5962/bhl.title.69024.

[2] P. Aumond, V. Masson, C. Lac, B. Gauvreau, S. Dupont, M. Berengier, Including the drag effects of canopies: real case large-eddy simulation studies, Boundary-Layer Meteorol. 146 (2013) 65–80, https://doi.org/10.1007/s10546-012-9758-x.

[3] J.H. Balbi, F. Morandini, X. Silvani, J.B. Filippi, F. Rinieri, A physical model for wildland fires, Combust. Flame 156 (2009) 2217–2230, https://doi.org/10.1016/j.combustflame.2009.07.010.

[4] T. Bergot, J. Escobar, V. Masson, Effect of small-scale surface heterogeneities and buildings on radiation fog: large-eddy simulation study at Paris–Charles de Gaulle airport, Q. J. R. Meteorol. Soc. 141 (2015) 285–298, https://doi.org/10.1002/qj.2358.

[5] A.S. Bova, W.E. Mell, C.M. Hoffman, A comparison of level set and marker methods for the simulation of wildland fire front propagation, Int. J. Wildland Fire 25 (2015) 229–241, https://doi.org/10.1071/WF13178.

[6] T.L. Clark, M.A. Jenkins, J. Coen, D. Packham, A coupled atmosphere–fire model: convective feedback on fire-line dynamics, J. Appl. Meteorol. Climatol. 35 (1996) 875–901.

[7] C.B. Clements, A.K. Kochanski, D. Seto, B. Davis, C. Camacho, N.P. Lareau, J. Contezac, J. Restaino, W.E. Heilman, S.K. Krueger, B. Butler, R.D. Ottmar, R. Vihnanek, J. Flynn, J.B. Filippi, T. Barboni, D.E. Hall, J. Mandel, M.A. Jenkins, J. O'Brien, B. Hornsby, C. Teske, The FireFlux II experiment: a model-guided field experiment to improve understanding of fire-atmosphere interactions and fire spread, Int. J. Wildland Fire 28 (2019) 308–326.

[8] C.B. Clements, B.E. Potter, S. Zhong, In situ measurements of water vapor, heat, and CO2 fluxes within a prescribed grass fire, Int. J. Wildland Fire 15 (2006) 299–306, https://doi.org/10.1071/WF05101.

[9] C.B. Clements, S. Zhong, X. Bian, W.E. Heilman, D.W. Byun, First observations of turbulence generated by grass fires, J. Geophys. Res.: Atmospheres 113 (2008), https://doi.org/10.1029/2008JD010014.

[10] C.B. Clements, S. Zhong, S. Goodrick, J. Li, B.E. Potter, X. Bian, W.E. Heilman, J. J. Charney, R. Perna, M. Jang, D. Lee, M. Patel, S. Street, G. Aumann, Observing the dynamics of wildland grass fires, Bull. Am. Meteorol. Soc. (2007), https://doi.org/10.1175/BAMS-88-9-1369.

[11] J. Coen, M. Cameron, J. Michalakes, E. Patton, P. Riggan, K. Yedinak, Wrf-fire: coupled weather–wildland fire modeling with the weather research and forecasting model, J. Appl. Meteorol. Climatol. 52 (2013) 16–38.

[12] J.L. Coen, W. Schroeder, S. Conway, L. Tarnay, Computational modeling of extreme wildland fire events: a synthesis of scientific understanding with applications to forecasting, land management, and firefighter safety, URL: J. Comput. Sci. 45 (2020) 101152. doi:10.1016/j.jocs.2020.101152, https://www.sciencedirect.com/science/article/pii/S1877750320304531.

[13] J.L. Coen, W. Schroeder, B. Quayle, The generation and forecast of extreme winds during the origin and progression of the 2017 tubbs fire, URL: Atmosphere 9

(2018). doi:10.3390/atmos9120462, https://www.mdpi.com/2073-4433/9/12/462.
[14] J.L. Coen, E.N. Stavros, J.A. Fites-Kaufman, Deconstructing the king megafire, URL: Ecol. Appl. 28 (2018) 1565–1580, https://doi.org/10.1002/eap.1752. arXiv: https://esajournals.onlinelibrary.wiley.com/doi/pdf/10.1002/eap.1752, https://esajournals.onlinelibrary.wiley.com/doi/abs/10.1002/eap.1752.
[15] P. Colella, P.R. Woodward, The piecewise parabolic method (PPM) for gas-dynamical simulations, J. Comput. Phys. 54 (1984) 174–201, https://doi.org/10.1016/0021-9991(84)90143-8.
[16] M.G. Cruz, M.E. Alexander, A.L. Sullivan, J.S. Gould, M. Kilinc, Assessing improvements in models used to operationally predict wildland fire rate of spread, Environ. Model. Software 105 (2018) 54–63, https://doi.org/10.1016/j.envsoft.2018.03.027.
[17] J. Cuxart, P. Bougeault, J.L. Redelsperger, A turbulence scheme allowing for mesoscale and large-eddy simulations, Q. J. R. Meteorol. Soc. 126 (2000) 1–30.
[18] J.B. Filippi, F. Bosseur, C. Mari, C. Lac, Simulation of a large wildfire in a coupled fire-atmosphere model, Atmosphere 9 (2018), https://doi.org/10.3390/atmos9060218.
[19] J.B. Filippi, F. Bosseur, C. Mari, C. Lac, P. Le Moigne, B. Cuenot, D. Veynante, D. Cariolle, J.H. Balbi, Coupled atmosphere-wildland fire modelling, J. Adv. Model. Earth Syst. 1 (2009), https://doi.org/10.3894/JAMES.2009.1.11.
[20] J.B. Filippi, F. Morandini, J.H. Balbi, D.R.C. Hill, Discrete event front-tracking simulation of a physical fire-spread model, Simulat. Trans. Soc. Model. Simul. Int. 87 (2011) 555–580.
[21] J.B. Filippi, X. Pialat, C.B. Clements, Assessment of ForeFire/Meso-NH for wildland fire/atmosphere coupled simulation of the FireFlux experiment, Proc. Combust. Inst. 34 (2013) 2633–2640.
[22] M.A. Finney, FARSITE: Fire Area Simulator – Model Development and Evaluation, Technical Report, US Department of Agriculture, Forest Service, Rocky Mountain Research Station, 1998.
[23] M. Fromm, D.T. Lindsey, R. Servranckx, G. Yue, T. Trickl, R. Sica, P. Doucet, S. Godin-Beekmann, The untold story of pyrocumulonimbus, Bull. Am. Meteorol. Soc. 91 (2010) 1193–1210, https://doi.org/10.1175/2010BAMS3004.1.
[24] R.J. Hodrick, E.C. Prescott, Postwar U.S. Business cycles: an empirical investigation, J. Money Credit Bank. 29 (1997) 1–16. URL: http://www.jstor.org/journals/ohio.press.html.
[25] G.S. Jiang, C.W. Shu, Efficient implementation of weighted ENO schemes, J. Comput. Phys. 126 (1996) 202–228, https://doi.org/10.1006/jcph.1996.0130.
[26] A.K. Kochanski, M.A. Jenkins, J. Mandel, J.D. Beezley, C.B. Clements, S. Krueger, Evaluation of WRF-SFIRE performance with field observations from the FireFlux experiment, Geosci. Model Dev. (GMD) 6 (2013) 1109–1126, https://doi.org/10.5194/gmd-6-1109-2013.
[27] A.K. Kochanski, M.A. Jenkins, J. Mandel, J.D. Beezley, S.K. Krueger, Real time simulation of 2007 Santa Ana fires, For. Ecol. Manag. 294 (2013) 136–149, https://doi.org/10.1016/j.foreco.2012.12.014.
[28] A.K. Kochanski, S.K. Krueger, M.A. Jenkins, J. Mandel, J.D. Beezley, Coupled Atmosphere-Fire Simulations of Fireflux: Impacts of Model Resolution on Model Performance, 2011 arXiv:1112.0494. AMS, Ninth Symposium on Fire and Forest Meteorology, Palm Springs.
[29] C. Lac, V. Masson, B. Aouizerats, C. Augros, P. Aumond, O. Caumont, J. Colin, F. Couvreux, J. Cuxart, G. Delautier, V. Ducrocq, O. Geoffroy, R. Honnert, J. Lafore, C. Brossier, Q. Libois, T. Maric, O. Nuissier, P. Peyrillé, J. Pergaud, E. Perraud, D. Ricard, S. Riette, Q. Rodier, R. Schoetter, J. Stein, M. Taufour, O. Thouron, S. Turner, A. Verrelle, B. Vié, F. Visentin, V. Vionnet, J. Chaboureau, J. Pinty, J. Escobar, M. Leriche, P. Bechtold, S. Berthet, J. Cohard, T. Dauhut, D. Gazen, F. Gheusi, C. Mari, P. Mascart, M. Mogé, G. Molinié, F. Pantillon, E. Richard, L. Seyfried, K. Suhre, P. Wautelet, P. Tulet, C. Barthe, S. Bielli, J. Pianezze, F. Auguste, T. Lunet, F. Bosseur, J. Filippi, J. Redelsperger, Overview of the Meso-NH model version 5.4 and its applications, Geosci. Model Dev. (GMD) 11 (2018) 1929–1969, https://doi.org/10.5194/gmd-11-1929-2018.
[30] J.P. Lafore, J. Stein, N. Asencio, P. Bougeault, V. Ducrocq, J. Duron, C. Fischer, P. Héreil, P. Mascart, V. Masson, J.P. Pinty, J.L. Redelsperger, E. Richard, J.V.G. de Arellano, The Meso-NH Atmospheric Simulation System. Part I: Adiabatic Formulation and Control Simulations, Annales Geophysicae, 1998, pp. 90–109, https://doi.org/10.1007/s00585-997-0090-6.
[31] C. Lautenberger, Wildland fire modeling with an eulerian level set method and automated calibration, Fire Saf. J. 62 (2013) 289–298.
[32] J. Mandel, J.D. Beezley, A.K. Kochanski, Coupled atmosphere-wildland fire modeling with WRF 3.3 and SFIRE 2011, Geosci. Model Dev. (GMD) 4 (2011) 591–610, https://doi.org/10.5194/gmd-4-591-2011.
[33] J. Mandel, J.D. Beezley, A.K. Kochanski, V.Y. Kondratenko, M. Kim, Assimilation of perimeter data and coupling with fuel moisture in a wildland fire-atmosphere DDDAS, Procedia Comput. Sci. 9 (2012) 1100–1109, https://doi.org/10.1016/j.procs.2012.04.119.
[34] V. Masson, P. Le Moigne, E. Martin, S. Faroux, A. Alias, R. Alkama, S. Belamari, A. Barbu, A. Boone, F. Bouyssel, P. Brousseau, E. Brun, J.C. Calvet, D. Carrer, B. Decharme, C. Delire, S. Donier, K. Essaouini, A.L. Gibelin, H. Giordani, F. Habets, M. Jidane, G. Kerdraon, E. Kourzeneva, M. Lafaysse, S. Lafont, C. Lebeaupin Brossier, A. Lemonsu, J.F. Mahfouf, P. Marguinaud, M. Mokhtari, S. Morin, G. Pigeon, R. Salgado, Y. Seity, F. Taillefer, G. Tanguy, P. Tulet, B. Vincendon, V. Vionnet, A. Voldoire, The SURFEXv7.2 land and ocean surface platform for coupled or offline simulation of Earth surface variables and fluxes, Geosci. Model Dev. (GMD) 6 (2013) 929–960, https://doi.org/10.5194/gmd-6-929-2013.
[35] W.E. Mell, M.A. Jenkins, J. Gould, P. Cheney, A physics-based approach to modelling grassland fires, Int. J. Wildland Fire 16 (2007) 1–22, https://doi.org/10.1071/WF06002.
[36] D. Muñoz-Esparza, B. Kosović, P.A. Jiménez, J.L. Coen, An accurate fire-spread algorithm in the weather research and forecasting model using the level-set method, J. Adv. Model. Earth Syst. 10 (2018) 908–926.
[37] J.J. O'Brien, E.L. Loudermilk, B. Hornsby, A.T. Hudak, B.C. Bright, M.B. Dickinson, J.K. Hiers, R.D. Ottmar, High-resolution infrared thermography for capturing wildland fire behaviour: RxCADRE 2012, Int. J. Wildland Fire 25 (2016) 62–75.
[38] S. Osher, R.P. Fedkiw, Level Set Methods and Dynamic Implicit Surfaces, ume 1, Springer, New York, 2003.
[39] S. Osher, J.A. Sethian, Fronts propagating with curvature-dependent speed: algorithms based on Hamilton-Jacobi formulations, J. Comput. Phys. 79 (1988) 12–49.
[40] S. Prichard, N.S. Larkin, R. Ottmar, N.H. French, K. Baker, T. Brown, C. Clements, M. Dickinson, A. Hudak, A. Kochanski, R. Linn, Y. Liu, B. Potter, W. Mell, D. Tanzer, S. Urbanski, A. Watts, The Fire and Smoke Model Evaluation Experiment – a plan for integrated, large fire–atmosphere field campaigns, Atmosphere 10 (2019), https://doi.org/10.3390/atmos10020066.
[41] R. Quill, J.J. Sharples, N.S. Wagenbrenner, L.A. Sidhu, J.M. Forthofer, Modeling wind direction distributions using a diagnostic model in the context of probabilistic fire spread prediction, Front. Mech. Eng. 5 (2019) 5, https://doi.org/10.3389/fmech.2019.00005.
[42] R.G. Rehm, R.J. McDermott, Fire Front Propagation Using the Level-Set Method, NIST, 2009. Technical Report 1611.
[43] M.C. Rochoux, C. Emery, S. Ricci, B. Cuenot, A. Trouvé, Towards predictive data-driven simulations of wildfire spread – Part II: ensemble Kalman Filter for the state estimation of a front-tracking simulator of wildfire spread, Nat. Hazards Earth Syst. Sci. 15 (2015) 1721–1739, https://doi.org/10.5194/nhess-15-1721-2015.
[44] M.C. Rochoux, S. Ricci, D. Lucor, B. Cuenot, A. Trouvé, Towards predictive data-driven simulations of wildfire spread – Part I: reduced-cost ensemble Kalman filter based on a polynomial chaos surrogate model for parameter estimation, Nat. Hazards Earth Syst. Sci. 14 (2014) 2951–2973, https://doi.org/10.5194/nhess-14-2951-2014.
[45] R.C. Rothermel, A Mathematical Model for Predicting Fire Spread in Wildland Fuels, Technical Report, U.S. Department of Agriculture, Forest Service, Intermountain forest and range experiment station, Ogden, Utah, USA, 1972.
[46] T. Sabatier, Y. Largeron, A. Paci, C. Lac, Q. Rodier, G. Canut, V. Masson, Semi-idealized simulations of wintertime flows and pollutant transport in an alpine valley. part ii: passive tracer tracking, Q. J. R. Meteorol. Soc. 146 (2020) 827–845, https://doi.org/10.1002/qj.3710.
[47] T. Sabatier, A. Paci, C. Lac, G. Canut, Y. Largeron, V. Masson, Semi-idealized simulations of wintertime flows and pollutant transport in an alpine valley: origins of local circulations (part i), Q. J. R. Meteorol. Soc. 146 (2020) 807–826, https://doi.org/10.1002/qj.3727.
[48] P.A. Santoni, J.B. Filippi, J.H. Balbi, F. Bosseur, Wildland fire behaviour case studies and fuel models for landscape-scale fire modeling, J. Combust. (2011) ID613424, https://doi.org/10.1155/2011/613424, 2011.
[49] J.A. Sethian, Theory, algorithms, and applications of level set methods for propagating interfaces, ANU 5 (1996) 309–395.
[50] W. Skamarock, J. Klemp, J. Dudhia, D. Gill, L. Zhiquan, J. Berner, W. Wang, J. Powers, M.G. Duda, D.M. Barker, X.Y. Huang, A Description of the Advanced Research Wrf Model Version 4, 145doi, NCAR Technical Note NCAR/TN-475+STR, 2019, https://doi.org/10.5065/1dfh-6p97.
[51] R.J. Sneeuwjagt, W.H. Frandsen, Behavior of experimental grass fires vs. predictions based on Rothermel's fire model, Can. J. For. Res. 7 (1977) 357–367.
[52] S. Strada, C. Mari, J.B. Filippi, F. Bosseur, Wildfire and the atmosphere: modelling the chemical and dynamic interactions at the regional scale, Atmos. Environ. 51 (2012) 234–249, https://doi.org/10.1016/j.atmosenv.2012.01.023.
[53] A.L. Sullivan, Wildland surface fire spread modeling, 1990-2007. 2: empirical and quasi-empirical models, Int. J. Wildland Fire 18 (2009) 369–386.
[54] V. Vionnet, E. Martin, V. Masson, C. Lac, F. Naaim Bouvet, G. Guyomarc'h, High-resolution large eddy simulation of snow accumulation in alpine terrain, J. Geophys. Res.: Atmospheres 122 (2017), https://doi.org/10.1002/2017JD026947, 11,5–11,021.
[55] C. Zhang, A. Collin, P. Moireau, A. Trouvé, M.C. Rochoux, State-parameter estimation approach for data-driven wildland fire spread modeling: application to the 2012 RxCADRE S5 field-scale experiment, Fire Saf. J. 105 (2019) 286–299, https://doi.org/10.1016/j.firesaf.2019.03.009.
[56] K. Zhang, S. Verma, A. Trouvé, A. Lamorlette, A study of the canopy effect on fire regime transition using an objectively defined Byram convective number, Fire Saf. J. 112 (2020) 102950, https://doi.org/10.1016/j.firesaf.2020.102950.
[57] Valéry Masson, Jean-Louis Champeaux, Fabrice Chauvin, Christelle Meriguet, Roselyne Lacaze, A global database of land surface parameters at 1-km resolution in meteorological and climate models, J. Clim. 16 (9) (2003) 1261–1282.